Title page

Rad5 and Rad51 act at telomeres through two partially distinct pathways

Running title: Rad5 function at telomeres

Erin E. Henninger[1], Pascale Jolivet[1], Prisca Berardi[1], Emilie Fallet[1], Mohcen Benmounah[1], Bechara Zeinoun[1], Gilles Charvin[2], Zhou Xu[1,#], Stefano Mattarocci[1,°,*] and Maria Teresa Teixeira[1,*]

[1] Sorbonne Université, PSL, CNRS, UMR8226, Institut de Biologie Physico-Chimique, Laboratoire de Biologie Moléculaire et Cellulaire des Eucaryotes, F-75005 Paris, France

[2] Université de Strasbourg, CNRS, UMR7156, Génétique Moléculaire, Génomique, Microbiologie, F-67000 Strasbourg, France

[#] Present address : Sorbonne Université, CNRS, UMR7238, Institut de Biologie Paris-Seine, Laboratory of Computational and Quantitative Biology, 75005 Paris, France

[°] Present address : DNA Repair and Chromosome Stability Team, Inserm U1274, Institut de Biologie François Jacob du Commissariat à l'Énergie Atomique et aux Énergies Alternatives, UMR E008 Université Paris-Saclay, Université de Paris, France

* correspondence to Stefano.mattarocci@inserm.fr; Teresa.teixeira@ibpc.fr

Abstract

Telomere maintenance relies on telomerase activity to compensate for the DNA end replication problem and on an efficient semi-conservative DNA replication machinery to traverse telomeric repetitive sequences, reputed to be hard to replicate. Here, we explore the telomeric functions of Rad5, a DNA helicase and ubiquitin ligase involved in the DNA damage tolerance (DDT) pathway. We show that Rad5 is enriched at telomeres mainly at the time of the passage of the replication fork. Among all the other DDT factors explored, only the removal of Rad5 showed an acceleration of senescence detected in population assays in the absence of telomerase. This early appearance of senescence detected in *rad5Δ* cells is compensated by a pathway involving the Rad51 recombinase and counteracted by the helicase Srs2, a pathway operating exclusively when telomeres become critically short. Rad51 binding at short telomeres is, at least partially, inhibited by Rad5. We propose that, independently of its role on the DDT pathway, Rad5 recruitment at replicating telomeres alters the ability of short telomeres to become substrates for Rad51 homology-dependent DNA repair.

Summary blurb

Rad5, which helps the replication fork to bypass replication road blocks, is found at telomeres at the time of their replication and may alter the ability of short telomeres to be substrates of Rad51.

Key words

Telomeres/DNA repair/DNA replication/Helicases/Telomerase/Replicative senescence

Main Text

Introduction

Telomeres cap the ends of eukaryotic chromosomes (Jain D & Cooper JP, 2010) and are composed of TG-rich repeat motifs of variable length. In budding yeast, telomeres have the degenerate sequence 5'-TG_{1-3}-3' and range from 200 to 400 bp in length, terminating in a 5-10 nt 3'-overhang on the strand running from the centromere to the telomere (Soudet J et al, 2014, Wellinger RJ & Zakian VA, 2012). The telomeric repeats recruit specific proteins to protect DNA ends from chromosome fusion and end degradation, by preventing the DNA damage response (DDR) at telomere ends. Telomeric proteins also control telomerase recruitment to chromosome ends. Without telomerase, telomeric DNA is lost at each passage of the replication fork, as the semiconservative replication machinery is unable to fully replicate the DNA ends.

In most human somatic tissues, which do not express telomerase, progressive telomere shortening is a major cause of senescence. Critically short telomeres activate a persistent DNA damage checkpoint; at the same time they prevent effective re-elongation by DNA repair activities (Campisi J & d'Adda dFF, 2007, Teixeira MT, 2013). Telomere-initiated senescence is bypassed in cancer cells by both suppressing the DNA damage checkpoint controlling replicative senescence and pathologically lengthening the telomeres (Artandi SE & DePinho RA, 2010, Shay JW & Wright WE, 2019).

Telomeric sequences share the characteristics of common fragile sites and pose similar problems for replication machinery, even in the absence of exogenous replication stress (Ivessa AS et al, 2002, Makovets S et al, 2004, Miller KM et al, 2006, Moore A et al, 2018, Sfeir A et al, 2009). Telomeres are difficult to replicate, likely because of secondary structures at telomeric repeats or interactions with telomeric components, such as the non-coding RNA TERRA or telomeric proteins (Douglas ME & Diffley JFX, 2021, Goto GH et al, 2015, Pfeiffer V et al, 2013, Voineagu I et al, 2009). Telomeres thus accumulate replication intermediates, which also recruit DNA repair factors. In yeasts, telomerase can efficiently re-

extend short or dysfunctional telomeric sequences, provided that a sufficient length of repeats is present (Matmati S et al, 2020, Miller KM et al, 2006, Negrini S et al, 2007, Strecker J et al, 2017, Vaurs M et al, 2022). Consequently, telomerase-negative cells become dependent on pathways responding to replication stress to maintain cell viability, probably by preventing abrupt telomere shortening events (Abdallah P et al, 2009, Fallet E et al, 2014, Jay KA et al, 2016, Lustig AJ, 2003). Yet, evidence from studies on mammalian cells suggest that telomeric replication intermediates require additional processing to promote telomerase access to restore telomere length and prevent toxic structures (Margalef P et al, 2018). In this situation, telomeric components likely modulate the access or the activity of fork remodeling factors at telomeres. Therefore, an intricate relationship exists between telomeric components, replication factors and DNA repair activities, but how they are coordinated remains unclear.

The DNA damage tolerance (DDT) pathway is an evolutionarily conserved pathway which aids DNA replication fork in bypassing DNA lesions (Arbel M et al, 2021a, Branzei D & Szakal B, 2016, Hoege C et al, 2002, Pfander B et al, 2005, Ulrich HD, 2011). The DDT pathway involves the Rad6/Rad18 ubiquitin ligase, which senses lesions. Rad6/Rad18 mono-ubiquitylates at least one subunit of Pol30 trimer (PCNA) at K164 which recruits Rad5 and stimulates translesion synthesis (TLS) by error-prone polymerases (Gallo D et al, 2019). However, the Rad5/Ubc13/Mms2 ubiquitin ligase can also poly-ubiquitylate mono-ubiquitinylated Pol30 at K164, leading to the error-free branch of the DDT pathway which results in a homology-mediated repair using the undamaged sister chromatid as a template. This pathway likely involves repriming DNA synthesis ahead of the lesion, leaving a single stranded DNA (ssDNA) gap. In current models of post-replicative template switching, the ssDNA gap is filled when the stalled nascent strand invades the newly synthesized sister strand for use as an undamaged template (Giannattasio M et al, 2014, Minca EC & Kowalski D, 2010). Alternatively, fork processing and restarting requires a replication fork reversal, a step involving Rad5 ATPase activity (Shin S et al, 2018). A series of distinct enzymatic activities and factors such as sister cohesion, helicases, recombinases, branch migration factors, DNA synthesis, endonucleases, and resolvases are involved in error-free DTT, but the exact choreography of events is unclear (Arbel M et al, 2021a, Ciccia A & Symington LS,

2016). Moreover, the kinetics and access of DNA repair factors to reaction intermediates are regulated. For instance, the PCNA trimer can also be sumoylated at K164 or K127 to recruit the Srs2 helicase, which removes Rad51 filaments needed for homology search and strand invasion (Arbel M et al, 2020, Lehmann CP et al, 2020). In this respect, the role of Rad51 recombinase and Rad52 in the process has been ambiguous, cooperating with DDT factors and acting in a so-called salvage pathway of the DDT, which becomes essential when template switching is deficient (Arbel M et al, 2021a, Ciccia A & Symington LS, 2016).

In this work we asked whether the DDT pathway acts at telomeres to assist in their replication. We demonstrate that the helicase/ubiquitin ligase Rad5 binds to telomeres during their replication. This function is not essential, since *RAD5* deletion is not lethal immediately after telomerase inhibition, as assessed by microfluidics experiments. In contrast, senescence rate measurements made in long-term cultures in the absence of telomerase indicate that Rad5 contributes to telomere maintenance and cell viability. The acceleration of senescence in the absence of Rad5 in these conditions is suppressed by absence of Srs2 in a Rad51-dependent manner, suggesting that Rad5 and Rad51 have partially independent activities at telomeres. Accordingly, Rad5, while potentially acting at telomeres of any length, limits the recruitment of Rad51 exclusively at short telomeres.

Results

Rad5 binds to telomeres during their replication

We and others previously reported that the ubiquitin ligase/helicase Rad5 binds to telomeres independent of their length and is required to sustain viability of telomerase-negative budding yeast cells (Claussin C & Chang M, 2016, Fallet E et al, 2014). We hypothesized that Rad5, involved in DDT pathway, could participate in the replication of telomeres, helping the fork to bypass replication barriers. To test this hypothesis, we determined whether Rad5 associates with telomeres during replication using chromatin immunoprecipitation (ChIP). We blocked cells in G1, then released them and followed their progression into S-phase (Figure 1A and supplementary Figure 1A). We monitored fork passage using ChIP for replication protein A (RPA) (Waga S & Stillman B, 1998). Consistent with previous reports (Hafner L et al, 2018, Mattarocci S et al, 2014), genomic regions corresponding to early and late origins fire at 45 and 60-75 min, respectively, after the release from the G1 block, while fork passage at two native telomeres (telomere 6R and 15L, containing a telomere-proximal subtelomeric X element and no Y' subtelomeric element) is at 90 min (Figure 1B and Supplementary Figure1B). We used the same ChIP samples to assess Myc-tagged Rad5 (Rad5-Myc) recruitment to telomeres. While we did not observe an enrichment of Rad5 at origins when they are fired, we did observe a Rad5 peak at the telomeres 6R and 15L at 90 min, which were absent in *rad5Δ* cells (Figure 1C and Supplementary Figure1C-E). Rad5 peaked at the same time as RPA at telomeres, suggesting that telomeres recruit additional Rad5 during replication, compared to other regions of the genome, perhaps because of their difficult replication.

Deletion of *RAD5* causes frequent cell death independently of telomerase activity

Defects in telomere replication, resulting in truncated telomeres, can be restored by telomerase (Chang M et al, 2007, Miller KM et al, 2006, Noel JF & Wellinger RJ, 2010), while, in the absence of telomerase, they may cause premature senescence, caused by the occurrence of at least one critically short telomere (Abdallah P et al, 2009, Ballew BJ & Lundblad V, 2013). These observations might explain why *RAD5* deletion leads to an accelerated loss of viability in the absence of telomerase (population assays; (Claussin C & Chang M, 2016, Fallet E et al, 2014) (see also Figure 4).

To precisely quantify the contribution of Rad5 to cell growth and senescence, we measured the number and the duration of the consecutive cell cycles of single cell lineages of *rad5Δ* cells in the presence or absence of telomerase using a microfluidics system (Xu Z et al, 2015) (Figure 2A). To inactivate telomerase, we switched the promoter of *TLC1*, encoding the telomerase template RNA component for TetO2, which is repressible by the addition of doxycycline in the media (Bah A et al, 2011). The expression of *TLC1* by TetO2 promoter (*PTetO2-TLC1*; doxycycline not added) had limited consequences on cell viability, regardless the presence of *RAD5* (Supplementary Figures 2A-D), although telomeres were shorter (260 bp on average (Xu Z et al, 2015)). On the other hand, deletion of *RAD5* in the presence of telomerase raised the mortality rate 20-fold (from ~0.2% and ~0.4% in *TLC1* and P_{TetO2}-*TLC1* to ~6%). Consequently, the average cell cycle duration increased from 76.9 ± 0.5 and 87.2 ± 0.5 min in *TLC1* and P_{TetO2}-*TLC1* to 105.3 ± 2.0 min (Supplementary Figure 2 C-D and Supplementary Table 1).

As expected, when telomerase was inactivated by addition of doxycycline in P_{tetO2}-*TLC1* cells, senescence phenotype became apparent with generations (Xu Z et al, 2015) (Supplementary Figure 2F). Deletion of *RAD5* in these conditions did have a strong effect, but not stronger as the one observed in *TLC1* cells, in which doxycycline has no effect on telomerase (Figure 2B-D and Supplementary Figure 2E). Therefore, telomerase inactivation in *rad5Δ* cells showed no obvious additional effect on viability during the first generations upon telomerase inactivation. We conclude that because the mortality rate in *rad5Δ* cells is substantially higher than the mortality resulting from telomerase inactivation, we cannot reach a definitive conclusion on the genetic interactions between *TLC1* and *RAD5* with this highly sensitive approach. Thus, the accelerated senescence measured in population assays upon telomerase inactivation is likely the result of the additivity of *rad5Δ* basal mortality and senescence-dependent mortality. Alternatively, the accelerated senescence measured in population assays may result from genetic interactions between telomerase and *RAD5* established on inherently more complex long-term cultures, typically when telomeres are shorter or when multiple cell cycles have been completed in the absence of both telomerase and Rad5.

Rad5 has a specific role at telomeres

Because the high mortality of *rad5*Δ cells is the dominant effect in microfluidics-based senescence study, we tested the effects of Rad5 separation-of-function mutations (Supplementary Figure 3A) on senescence rates using a cell population assay on solid media as previously described (Fallet E et al, 2014).

In accordance with previous results, the Rad5-GAA and Rad5-AA mutations in the helicase domain and Rad5-I916A mutation in the RING domain (Choi K et al, 2015) had smaller effect on UV and methyl methanesulfonate (MMS) sensitivity, compared to the full deletion of *RAD5* (Supplementary Figure 3B). These results indicate that, while displaying separation-of-function phenotypes in specific contexts, they behave as hypomorphs with respect to viability in cells challenged with genotoxic stresses (Ball LG et al, 2014, Gallo D et al, 2019, Gangavarapu V et al, 2006, Ortiz-Bazan MA et al, 2014). Moreover, these mutants, as well as the *RAD5* deletion, did not alter telomere length (Supplementary Figure 3C), nor had an effect on senescence timing in cells lacking *TLC1* (Figure 3A-C, Supplementary Figure 3D). Thus, the helicase and ubiquitin ligase functions of Rad5 do not seem to be essential in sustaining cell growth in the absence of telomerase. We hypothesize that telomerase inactivation could affect the cells in a similar manner as low dosage of MMS or UV, for which Rad5 hypomorph mutations have little or no effect on viability. This result is in accordance with the idea that the function of the full length Rad5 in replication is more important than the helicase or ubiquitin ligase biochemical activities taken separately, because Rad5 is also required for the recruitment of TLS polymerases (Gallo D et al, 2019).

Given that Rad5 plays a major role in DDT, we asked whether other DDT components could be involved in telomere maintenance, using the same senescence assays (Supplementary Figure 3E). Deletion of TLS polymerase subunits Rev1, Rev3 (polymerase zeta), or Rad30 (polymerase eta) did not accelerate senescence in *tlc1*Δ cells (Figure 3D and Supplementary Figure 3F-G). To understand the role of Pol30-K164 poly-ubiquitylation, we deleted *MMS2* and *UBC13*, which encode the other subunits of ubiquitin-conjugating enzyme complex (E2) that cooperates with Rad5. We observed a loss in cell viability upon challenge with UV or MMS; however, the effect was not as severe as for *RAD5* deletion (Supplementary Figure

3B). *mms2*Δ and *ubc13*Δ cells did not accelerate senescence in *tlc1*Δ cells (Figure 3E-F), confirming previous observations (Fallet E et al, 2014). PCNA can be also ubiquitylated on lysine K107 by Rad5 and Mms2 together with the E2 ligase Ubc4 (Das-Bradoo S et al, 2010). We asked whether other E2 ubiquitin ligases might have a function at telomeres together with Rad5. Neither *UBC4* deletion or *pol30-K107R* mutation accelerated the onset of senescence in *tlc1*Δ cells (Supplementary Figure 3H-J). Therefore, the mechanism of Rad5-dependent telomere protection does not seem to rely on Ubc4 or Pol30-K107 mono-ubiquitylation. Since the complete loss of *RAD5* had a larger effect on viability compared to the other DDT factors tested, it suggests that the combination of these activities or a yet undiscovered function of Rad5 might be important for the survival of telomerase-negative cells.

Rad5 and Rad51 have partially additive roles in the absence of telomerase

Rad51 also functions in the error-free DDT pathway, possibly contributing to strand invasion and annealing of parental strands at fork junctions or at ssDNA gaps (Arbel M et al, 2021a, Branzei D & Szakal B, 2017, Liberi G et al, 2005). However, in budding yeast, Rad51 activity at replicative forks is restrained by the helicase Srs2 to prevent aberrant Rad51-dependent recombination. Srs2 is recruited to replicative forks by the sumoylation of PCNA, principally at lysine 164 (Arbel M et al, 2020, Hoege C et al, 2002) (Supplementary Figure 3E). *SRS2* deletion suppresses genotoxic sensitivity caused by *RAD5* deletion (Broomfield S & Xiao W, 2002, Friedl AA et al, 2001, Ulrich HD, 2001). Rad51 is critical for viability of cells in which telomerase is inactivated (Ballew BJ & Lundblad V, 2013, Fallet E et al, 2014, Le S et al, 1999, Lundblad V & Blackburn EH, 1993, Xu Z et al, 2015). While its role in post-senescence survival and inter-telomeric recombination is well established, the function of Rad51, or of homology-directed repair in general, at telomeres early after telomerase inactivation is unclear (Ballew BJ & Lundblad V, 2013, Claussin C & Chang M, 2015; 2016, Xu Z et al, 2015).

We asked whether Rad51 contributes to telomere maintenance through its role in DDT. To test this idea, we checked whether the genetic interactions between *rad5Δ, srs2Δ,* and *pol30–K164R* mutations seen during genotoxic exposure could be recapitulated in the absence of telomerase.

Firstly, we checked that *pol30-K164R* conferred UV sensitivity to WT cells similar to *rad5Δ*, and that the *rad5Δ pol30-K164R* double mutant was nearly epistatic to *rad5Δ* (Supplementary Figure 4A). In contrast, *srs2Δ* did not affect cells exposed to UV, but completely suppressed *rad5Δ* defects. These results are consistent with the current model of DDT. Indeed, both the Pol30-K164 ubiquitylation-dependent error-prone and Rad5-dependent error-free pathways are required for full cell viability upon genotoxic exposure, whereas *SRS2* deletion allows unrestrained Rad51 action, compensating for Rad5 inactivation (Supplementary Figure 3E).

We then checked the cell viability in the absence of telomerase for these genotypes. *pol30-K164R* had no effect on cell viability in the absence of telomerase, in contrast to UV exposure, and didn't alter the effect of *RAD5* deletion (Figure 4A). In contrast, *SRS2* deletion suppressed the effect of *RAD5* deletion (Figure 4B and D), as seen with UV exposure. This suggests that sumoylation of PCNA and recruitment of Srs2 play a role at telomeres. Consistently, the *srs2-ΔSIM* (Miura T et al, 2013) mutant, which lacks the C-terminal portion of Srs2 containing both the PCNA interaction motif (PIP) and a SUMO-interaction motif (SIM), also suppressed the phenotype of *rad5Δ* (Figure 4C and Supplementary Figure 4B). *srs2Δ* suppression of *rad5Δ* defects rely on *RAD51*, since *tlc1Δ rad5Δ srs2Δ rad51Δ* cells grew extremely poorly (Figure 4D). These data support the idea that PCNA sumoylation and Srs2 recruitment could repress Rad51 activity. Furthermore, *rad5Δ* and *rad51Δ* had additive effects in the *tlc1Δ* background, despite the presence of Srs2 (Figure 4D). Thus, Rad51 is likely to play a critical role at telomeres in *rad5Δ* cells when not inhibited by Srs2. Alternatively, Rad5 and Rad51 may act on two partially non-overlapping pathways at telomeres, independently of Srs2. One hypothesis is that telomeres in *rad5Δ* cells may become appropriate substrates of Rad51, even in the presence of Srs2 (see below).

Srs2 and Rad5 limit Rad51 recruitment to critically short telomeres

Our genetic data suggest Rad51 is prevented from rescuing defects at telomeres in *rad5Δ* cells by the action of Srs2. We thus asked whether Rad51 recruitment to telomeres depends on Rad5 and/or Srs2, using ChIP assay. Because Rad51 is detected only at critically short telomeres (Fallet E et al, 2014), we engineered our strains to stably harbor an inducible very short telomere (Diede SJ & Gottschling DE, 1999, Michelson RJ et al, 2005, Ribeyre C &

Shore D, 2012). A chromosome end containing 80 bp (TG80, critically short) or 250 bp (TG250, control length telomeres) of telomeric repeats was generated *de novo*. This is achieved upon incubation of cells in media containing galactose, in which the endonuclease HO is experimentally induced to generate a double-strand break close to a stretch of 80 or 250 bp of telomeric repeats (Figure 5A and Supplementary Figure 5A). We also inhibited telomerase, which would otherwise re-elongate the newly generated critically short telomere, by adding doxycycline in the P_{TetO2}-TLC1 background. These constructs were combined in strains containing *RAD5* and *SRS2* deletions and ChIP experiments were performed using an anti-Rad51 antibody.

Consistent with previous results (Fallet E et al, 2014), Rad51 was recruited only at critically short telomeres (TG80) in the *RAD5 SRS2* background and further recruited in absence of Srs2 (Figure 5B and Supplementary Figure 5B). Surprisingly, the deletion of *RAD5* gene increased the Rad51 recruitment at short telomere (TG80). These ChIP results indicate that both Rad5 and Srs2 presence is required to fully prevent Rad51 recruitment to short telomeres. This is consistent with our hypothesis that, in absence of Rad5, telomeres may become better substrates of Rad51, even in the presence of the known Rad51-suppressor Srs2. In the absence of both *RAD5* and *SRS2*, binding of Rad51 to TG80 was further increased, compared to *rad5Δ* cells, but was not significantly different from the binding seen in *srs2Δ* cells (Figure 5B and Supplementary Figure 5B). This suggests that Rad5 and Srs2 exert redundant, partially independent activities in preventing Rad51 accumulation at telomeres, with Srs2 exerting a greater effect. In the same cells, a native telomere (tel6R) did not bind Rad51, in any of the mutants. We did not see accumulation of Rad51 at normal length telomeres in cells containing the TG250 telomere either, even in *srs2Δ rad5Δ* cells. We conclude that normal length functional telomeres are not substrates for Rad51, while both Rad5 and Srs2 are recruited to telomeres, mostly independently of their length (Figure 5C-D and Supplementary Figure 5C-D).

Discussion

In this work we show that Rad5, a component of the DNA damage tolerance pathway, associates with telomeres during replication suggesting a role in telomere replication. In telomerase-negative cells, the impact of *RAD5* deletion on growth, as assessed in long-term population cultures, can be compensated by the action of Rad51, which is itself restrained by Srs2. Rad51 can be detected at telomeres only when they reach a short length, and its binding to telomeres is restricted by both Rad5 and Srs2. In contrast, Srs2 and Rad5 are present at telomeres independently of their length. Thus, Rad5 and Rad51 contribute to at least two partially distinct pathways at telomeres.

Our results of microfluidics, where cells grow individually with no competition or selection of best growers, show that *RAD5* deletion causes ~6% of cell mortality (Figure 2). This mortality rate leads to a doubling time of *rad5Δ* cultures 1.3-1.4 greater than wild-type, (Supplementary Table 1 and (Gallo D et al, 2019, Johnson RE et al, 1992)), and a slight decrease in colony size. This growth defect is likely due to a constitutive role of Rad5 during normal S-phase in assisting replication along the overall genome in loci other than telomeres, and most *rad5Δ* defects in preventing DNA damage are known to be suppressed by *SRS2* deletion (Friedl AA et al, 2001, Liefshitz B et al, 1998). This effect causes premature cell death of cell lineages after a median of ~15 cell cycles after the start of recording or a median of ~5 additional cell cycles after addition of doxycycline. Therefore, *RAD5*'s deletion effect by microfluidics cannot be assessed on the long-term, when telomeres become extremely short, for instance when an effect of Rad5 on Rad51 recruitment at telomeres is detected (Figure 5 and Supplementary Figure 5). More generally, our observations highlight a general difficulty in interpreting the level of synthetic lethality interactions between two mutations showing slight defects in growth when taken separately, and showing dramatic effects when combined.

To explain that Rad5 and Rad51 have a role in distinct pathways, we can envisage that Rad5 and Rad51 promote cell growth in the absence of telomerase in different cells with different

telomere contents, and there may be no interaction between these two pathways at the molecular level. For instance, in highly heterogeneous senescent cultures, some cells may display critically short telomeres and require Rad51 for viability, whereas others may require Rad5 for independent reasons at telomeres or elsewhere in the genome. Cells requiring Rad51 would promote homology-dependent repair at the short telomeres, in response to extended 5'-3' resection of short telomeres (Fallet E et al, 2014). However, our results also suggest some overlap between Rad5 and Rad51 pathways: *SRS2* deletion suppresses *RAD5* deletion, and *RAD5* deletion affects the ability to Rad51 to bind telomeres (Figures 4-5). In this work, while we suggest that Rad5 accumulation at telomeres prevents Rad51 recruitment, we cannot exclude Rad5 or the DTT pathway being involved via distinct functionally redundant DDT branches in the Rad51-dependent processing of short telomeres, as shown for genotoxic stress (Gallo D et al, 2019). While the role of Rad5 and Rad51 in template switching and/or replication fork structures is not well understood (Arbel M et al, 2021b, Branzei D & Szakal B, 2016), we observed that Rad5 itself was not required for Rad51 binding to short telomeres. Instead, short telomeres in *rad5Δ* cells are bound by more Rad51 (Figure 5 and Supplementary Figure 5). One possible explanation to all these data would be that short telomeres in the absence of Rad5 become better substrates for Rad51 binding. How Rad5 affects the structure of telomeres is yet to be determined.

Materials and Methods

Yeast strains

All strains used in this work are in a W303 *RAD5 ADE2* background (Supplementary Table 2). Gene deletions and epitope-tagging were constructed as described (Longtine MS et al, 1998). Point mutations were constructed by a two-step strategy. First, a marker (*HIS3MX6* or *kLEU2*) was first inserted in the 3'-UTR of the target gene. Then a construct was amplified using a reverse primer downstream of the inserted marker, and a forward primer containing the desired mutation for the target gene. The PCR construct was used to transform naïve cells, and clones were selected with Histidine or Leucine dropout plates (Toulmay A & Schneiter R, 2006). Primers used are listed in Supplementary Table 3.

Cell synchronization and Flow Cytometry

The strains used were *MAT***a** *bar1*Δ, and an overnight culture of each was diluted about 10-fold into 540 ml of YPD. After 3.5 hr growth at 30°C, **α** factor (Bachem) was added to a final concentration of 10^{-7} M and cultures were incubated for 130 minutes at 30°C. For the release, cells were washed three times in H_20, then treated with nuclease-free Pronase (Millipore; 46 mg total), and placed in 540 ml YPD medium at 18°C. Samples were taken every 15 minutes for ChIP and flow cytometry analysis. Cell-cycle synchrony and release were checked by microscope. Cytometry analysis of the DNA content was performed using Ethanol-fixed cells and Sytox Green (Invitrogen) staining. Analysis was performed on the Accuri C6. Data was graphed using MATLAB.

Chromatin Immunoprecipitation

ChIP was performed as previously described (Mattarocci S et al, 2014). For each ChIP culture, 40 mL of cells (at about 10^7 cells/mL) were fixed in 1% formaldehyde for 5 minutes, then the reaction was stopped with 2 mL 2.5 M glycine. Next, cells were washed with ice cold HBS twice [HBS: 50 mM HEPES pH 7.8, 140 mM NaCl], and frozen in 600 µL of ChIP lysis buffer plus with protease inhibitors and 1 mM PMSF (Roche 11836170001) [ChIP lysis buffer: 50 mM HEPES pH 7.8, 140 mM NaCl, 1 mM EDTA, 1% NP40, 1% Sodium deoxycholate]. Cells were lysed using a FastPrep (MP Biomedicals), 3x30 seconds at 6 M/s

and zirconium/silica beads (BioSpec Products 11079105z). Next, beads were removed from lysates by using a needle to poke a hole in the tube and spinning the sample into a clean tube. Supernatant and pellet were resuspended in 600 µL lysis buffer and protease inhibitors, and samples were sonicated at high setting, 30″ on 30″ off for 10′ using a Diagenode with continuously cooled water bath at 4°C. Sonicates were clarified by spinning top speed for 30′ at 4°C. Immunoprecipitations were set up with either anti Myc (9E10 from hybridoma culture supernatant (gift from David Shore's lab), anti-Rad51 (Abcam ab63798), or anti-RPA (polyclonal Agrisera AS07214 directed against the three RPA subunits). After 1 hr of incubation at 4 °C with rotation with antibody, either sheep anti-mouse (Invitrogen: 11201D) or sheep anti-rabbit (Invitrogen: 11203D) beads were added and incubated for 2 hours at 4°C with rotation. For washes, samples were placed on a magnet to collect beads. Beads were first rinsed in 1 mL ChIP lysis buffer and transferred to a new tube. Then, beads were washed with AT1, AT2, AT3, and AT4 wash buffers [AT1: 50 mM HEPES pH 7.8, 140 mM NaCl, 1mM EDTA, 0.03% SDS (added freshly); AT2: 50 mM HEPES pH 7.8, 1M NaCl, 1 mM EDTA; AT3: 20 mM Tris, 250 mM LiCl, 1 mM EDTA, 0.5% NP40, 0.5% Sodium deoxycholate; AT4: 20 mM Tris pH 7.5, 0.1 mM EDTA]. After washes, samples were eluted in 140 µL of elution buffer (AT4 + 1% SDS). Samples, including 10 µL of each input, were reverse crosslinked overnight in 140 µL elution buffer at 65°C. The next day, samples were digested in proteinaseK/TE for 1 hour at 37°C, and then cleaned-up using a QIAquick PCR Purification Kit (Qiagen 28104). qPCR was performed in a 10 µL volume with PowerSYBR green PCR master mix (Applied Biosystems 4367659) on the Applied Biosystems. The program used for the reactions is: 95°C for 10 min, then a 44x loop of 95°C 15 sec, 60°C for 1 min. Primers are listed in Supplementary Table 3. Percent input was calculated by the equation percent input = $(E)^{Ct(input)-Ct(IP)}$, where E is the PCR efficiency of the primer set. The $Ct_{(input)}$ was first corrected for dilution by the formula $Ct' = Ct - \log_E(30)$.

Microfluidics analyses

Microfluidics analyses were adapted from (Xu Z et al, 2015). The microfluidic mold was fabricated using standard soft lithography techniques. In brief, polydimethylsiloxane (PDMS; Sylgard 184) and curing agent were mixed in a 10:1 ratio, degassed it with a vacuum pump for 30′, and poured it into the mold. The PDMS was cured by baking at 70 °C for 5 h and then removed from the mold. A biopsy puncher (1.5 mm, Harris Unicore) was used to create

holes for medium flow. The surfaces of PDMS and a glass coverslip (24 × 50 mm) were surface activated using a plasma cleaner (Diener Electronic, Germany) to covalently bond the two elements. For injection of cells into the device, synthetic complete medium containing 2% glucose (SD) was filtered using a 0.22-μm polyethersulfone filter (Corning) and loaded into the device using a peristaltic pump (IPCN, Ismatec). Cells from a log-phase culture (0.5 OD_{600}) were injected into the device using a 1 ml syringe. A constant medium flow (28 μl/min) was maintained throughout the experiment. For experiments with strains expressing the TetO2-*TLC1* construct, cells were allowed to divide and invade the cavities for 12–24 h before the medium was switched to SD containing 30 μg/ml doxycycline. Cells in the microfluidic device were imaged using a fully motorised Axio Observer Z1 inverted microscope (Zeiss), with constant focus maintained with focus stabilisation hardware (Definite focus, Zeiss). LED light sources for phase contrast were used with the following parameters: 4.0 V – 70 ms. The temperature was maintained at 30 °C with a controlled heating unit and an incubation chamber that held the entire microscope base, including the stage and the objectives. Images were acquired every 10′ using 4Zen (Zeiss). A custom software written in Matlab, named SingleCellTracer, was developed in this work to allow a semi-automated analysis of cell division dynamics of individual lineages. In brief, an input microscopy movie can be directly analyzed through the user interface allowing manual detection of cell budding, divisions, as well as correction of mistakes and simultaneous monitoring of several features over time. Time-lapse images were exported as avi files and analysed directly with the graphical user interface of SingleCellTracer. To efficiently track lineages, in which we frequently switched focus from a given cell to its daughter cell, the time-lapse images were retrospectively analysed starting from the last image. This avoided tracking of lineages in which the cells were ejected from the microcavity. All computational and statistical analyses were performed in Matlab. SingleCellTracer and the functions developed in this study are available on request.

Quantitative senescence assays

Senescence assays and their analysis were performed as previously described (Fallet E et al, 2014). Briefly, diploids heterozygous for the relevant genes and containing a *TLC1* deletion replaced by a *Mat***α** specific Nourseothricin (Nat) reporter (*PralphaNat*) were sporulated and germinated on Nat for selection of telomerase-negative spores. Genotypes were

determined on a small portion of the colony, and 8 to 16 clones of each genotype were spotted on YPD supplemented with Nourseothricin (50,000 cells in the first spot, followed by 10-fold serial dilutions). After 46 hours at 30°C, plates were scanned (Passage 1). Cells were then picked from the most concentrated spot, to re-spot as previously for Passage 2. Passage 3 was obtained in the same manner with cells from Passage 2. Spot intensity was measured from scans after 46 h of growth and used to determine a viability index (corresponding to the dilution required to reach a given intensity threshold) using ImageJ 1.46a. Viability indexes for each genotype were plotted as boxplots using MATLAB. p-values were determined using pairwise Wilcoxon rank-sum tests in MATLAB (*= $p < .05$; ** = $p < .005$). At least two complete and biological independent experiments using independent transformants were performed for each pair of diploid starting strains and one is shown.

Southern Blotting

Southern blot analysis was performed using 250 ng of DNA from each strain. DNA was digested with *Xho* I, separated on a 1.2% agarose gel, and transferred to Hybond-XL membrane. The blots were probed with a 1 kb probe for Y'-prime elements. The primers used to make the probe were Fwd: 5'- GAGTTTTTCAGCGTTTGCGTTCCA-3' Rev: 5'-TTACTCTCGCTGTCACTCCTTACC-3'. The membranes were hybridized in Church buffer at 65°C overnight, and washed four times in Church wash buffer [Church buffer: 500 mM sodium phosphate pH 7.4, 1 mM EDTA; 7% SDS, 1% BSA; Church wash buffer: 20 mM sodium phosphate pH 7.4, 1 mM EDTA, 1% SDS].

Acknowledgements

We wish to thank D. Shore, M. Lisby, E. Bonnel and R. Wellinger for sharing strains, reagents and technical advice and G. Riddihough from Life Science Editors for help editing the manuscript. We also thank the Teixeira lab and of the UMR8226 unit members for technical support and fruitful discussions. Work in MTT lab was supported by the European Research Council (ERC- 2010-StG 260906—D-END), the Mairie de Paris (Programme Emergences), the "Fondation de la Recherche Medicale" ("équipe labellisée"), by the French National Research Agency (ANR) as part of the "Investissements d'Avenir" Program (LabEx Dynamo ANR-11-LABX-0011-01) and ANR-16-CE12-0026, and the "Institut National du Cancer (INCa_15192). EH and PB were supported by a fellowship from the Ligue Contre le Cancer (France). ZX is supported by ANR grant ANR-17-CE20-0002-01 and Mairie de Paris (Programme Emergences).

Conflict of Interest

The authors declare no conflict of interest

References

Abdallah P, Luciano P, Runge KW, Lisby M, Geli V, Gilson E, Teixeira MT (2009) A two-step model for senescence triggered by a single critically short telomere. *Nature cell biology* 11: 988-993. doi:10.1038/ncb1911

Arbel M, Bronstein A, Sau S, Liefshitz B, Kupiec M (2020) Access to pcna by srs2 and elg1 controls the choice between alternative repair pathways in saccharomyces cerevisiae. *mBio* 11: doi:10.1128/mBio.00705-20

Arbel M, Choudhary K, Tfilin O, Kupiec M (2021a) Pcna loaders and unloaders-one ring that rules them all. *Genes* 12: doi:10.3390/genes12111812

Arbel M, Liefshitz B, Kupiec M (2021b) DNA damage bypass pathways and their effect on mutagenesis in yeast. *FEMS Microbiol Rev* 45: doi:10.1093/femsre/fuaa038

Artandi SE, DePinho RA (2010) Telomeres and telomerase in cancer. *Carcinogenesis* 31: 9-18. doi:10.1093/carcin/bgp268

Bah A, Gilson E, Wellinger RJ (2011) Telomerase is required to protect chromosomes with vertebrate-type t2ag3 3' ends in saccharomyces cerevisiae. *The Journal of biological chemistry* 286: 27132-27138. doi:10.1074/jbc.M111.220186

Ball LG, Xu X, Blackwell S, Hanna MD, Lambrecht AD, Xiao W (2014) The rad5 helicase activity is dispensable for error-free DNA post-replication repair. *DNA Repair (Amst)* 16C: 74-83. doi:10.1016/j.dnarep.2014.02.016

Ballew BJ, Lundblad V (2013) Multiple genetic pathways regulate replicative senescence in telomerase-deficient yeast. *Aging Cell*: doi:10.1111/acel.12099

Branzei D, Szakal B (2016) DNA damage tolerance by recombination: Molecular pathways and DNA structures. *DNA Repair (Amst)* 44: 68-75. doi:10.1016/j.dnarep.2016.05.008

Branzei D, Szakal B (2017) Building up and breaking down: Mechanisms controlling recombination during replication. *Crit Rev Biochem Mol Biol* 52: 381-394. doi:10.1080/10409238.2017.1304355

Broomfield S, Xiao W (2002) Suppression of genetic defects within the rad6 pathway by srs2 is specific for error-free post-replication repair but not for damage-induced mutagenesis. *Nucleic Acids Res* 30: 732-739.

Campisi J, d'Adda dFF (2007) Cellular senescence: When bad things happen to good cells. *Nat Rev Mol Cell Biol* 8: 729-740. doi:10.1038/nrm2233

Chang M, Arneric M, Lingner J (2007) Telomerase repeat addition processivity is increased at critically short telomeres in a tel1-dependent manner in saccharomyces cerevisiae. *Genes Dev* 21: 2485-2494.

Choi K, Batke S, Szakal B, Lowther J, Hao F, Sarangi P, Branzei D, Ulrich HD, Zhao X (2015) Concerted and differential actions of two enzymatic domains underlie rad5 contributions to DNA damage tolerance. *Nucleic Acids Res* 43: 2666-2677. doi:10.1093/nar/gkv004

Ciccia A, Symington LS (2016) Stressing out about rad52. *Mol Cell* 64: 1017-1019. doi:10.1016/j.molcel.2016.11.036

Claussin C, Chang M (2015) The many facets of homologous recombination at telomeres. *Microbial cell (Graz, Austria)* 2: 308-321. doi:10.15698/mic2015.09.224

Claussin C, Chang M (2016) Multiple rad52-mediated homology-directed repair mechanisms are required to prevent telomere attrition-induced senescence in saccharomyces cerevisiae. *PLoS Genet* 12: e1006176. doi:10.1371/journal.pgen.1006176

Coutelier H, Xu Z, Morisse MC, Lhuillier-Akakpo M, Pelet S, Charvin G, Dubrana K, Teixeira MT (2018) Adaptation to DNA damage checkpoint in senescent telomerase-negative cells promotes genome instability. *Genes Dev* 32: 1499-1513. doi:10.1101/gad.318485.118

Das-Bradoo S, Nguyen HD, Bielinsky AK (2010) Damage-specific modification of pcna. *Cell Cycle* 9: 3674-3679. doi:13121 [pii]

10.4161/cc.9.18.13121 [doi]

Diede SJ, Gottschling DE (1999) Telomerase-mediated telomere addition in vivo requires DNA primase and DNA polymerases alpha and delta. *Cell* 99: 723-733.

Douglas ME, Diffley JFX (2021) Budding yeast rap1, but not telomeric DNA, is inhibitory for multiple stages of DNA replication in vitro. *Nucleic Acids Research*: doi:10.1093/nar/gkab416

Fallet E, Jolivet P, Soudet J, Lisby M, Gilson E, Teixeira MT (2014) Length-dependent processing of telomeres in the absence of telomerase. *Nucleic acids research* 42: 3648-3665. doi:10.1093/nar/gkt1328

Friedl AA, Liefshitz B, Steinlauf R, Kupiec M (2001) Deletion of the srs2 gene suppresses elevated recombination and DNA damage sensitivity in rad5 and rad18 mutants of saccharomyces cerevisiae. *Mutation Research* 486: 137-146. doi:S0921877701000866 [pii]

Gallo D, Kim T, Szakal B, Saayman X, Narula A, Park Y, Branzei D, Zhang Z, Brown GW (2019) Rad5 recruits error-prone DNA polymerases for mutagenic repair of ssdna gaps on undamaged templates. *Mol Cell*: doi:https://doi.org/10.1016/j.molcel.2019.01.001

Gangavarapu V, Haracska L, Unk I, Johnson RE, Prakash S, Prakash L (2006) Mms2-ubc13-dependent and -independent roles of rad5 ubiquitin ligase in postreplication repair and translesion DNA synthesis in saccharomyces cerevisiae. *Molecular and Cellular Biology* 26: 7783-7790. doi:MCB.01260-06 [pii] 10.1128/MCB.01260-06

Giannattasio M, Zwicky K, Follonier C, Foiani M, Lopes M, Branzei D (2014) Visualization of recombination-mediated damage bypass by template switching. *Nat Struct Mol Biol* 21: 884-892. doi:10.1038/nsmb.2888

Goto GH, Zencir S, Hirano Y, Ogi H, Ivessa A, Sugimoto K (2015) Binding of multiple rap1 proteins stimulates chromosome breakage induction during DNA replication. *PLoS Genet* 11: e1005283. doi:10.1371/journal.pgen.1005283

Hafner L, Lezaja A, Zhang X, Lemmens L, Shyian M, Albert B, Follonier C, Nunes JM, Lopes M, Shore D, et al (2018) Rif1 binding and control of chromosome-internal DNA replication origins is limited by telomere sequestration. *Cell Rep* 23: 983-992. doi:10.1016/j.celrep.2018.03.113

Hoege C, Pfander B, Moldovan GL, Pyrowolakis G, Jentsch S (2002) Rad6-dependent DNA repair is linked to modification of pcna by ubiquitin and sumo. *Nature* 419: 135-141. doi:10.1038/nature00991

Ivessa AS, Zhou JQ, Schulz VP, Monson EK, Zakian VA (2002) Saccharomyces rrm3p, a 5' to 3' DNA helicase that promotes replication fork progression through telomeric and subtelomeric DNA. *Genes Dev* 16: 1383-1396.

Jain D, Cooper JP (2010) Telomeric strategies: Means to an end. *Annual review of genetics* 44: 243-269. doi:10.1146/annurev-genet-102108-134841

Jay KA, Smith DL, Blackburn EH (2016) Early loss of telomerase action in yeast creates a dependence on the DNA damage response adaptor proteins. *Molecular and cellular biology* 36: 1908-1919. doi:10.1128/MCB.00943-15

Johnson RE, Henderson ST, Petes TD, Prakash S, Bankmann M, Prakash L (1992) Saccharomyces cerevisiae rad5-encoded DNA repair protein contains DNA helicase and zinc-binding sequence motifs and affects the stability of simple repetitive sequences in the genome. *Molecular and Cellular Biology* 12: 3807-3818.

Le S, Moore JK, Haber JE, Greider CW (1999) Rad50 and rad51 define two pathways that collaborate to maintain telomeres in the absence of telomerase. *Genetics* 152: 143-152.

Lehmann CP, Jiménez-Martín A, Branzei D, Tercero JA (2020) Prevention of unwanted recombination at damaged replication forks. *Curr Genet*: doi:10.1007/s00294-020-01095-7

Liberi G, Maffioletti G, Lucca C, Chiolo I, Baryshnikova A, Cotta-Ramusino C, Lopes M, Pellicioli A, Haber JE, Foiani M (2005) Rad51-dependent DNA structures accumulate at damaged replication forks in sgs1 mutants defective in the yeast ortholog of blm recq helicase. *Genes Dev* 19: 339-350.

Liefshitz B, Steinlauf R, Friedl A, Eckardt-Schupp F, Kupiec M (1998) Genetic interactions between mutants of the 'error-prone' repair group of saccharomyces cerevisiae and their effect on recombination and mutagenesis. *Mutation Research* 407: 135-145.

Longtine MS, McKenzie AI, Demarini DJ, Shah NG, Wach A, Brachat A, Philippsen P, Pringle JR (1998) Additional modules for versatile and economical pcr-based gene deletion and modification in saccharomyces cerevisiae. *Yeast* 14: 953-961.

Lundblad V, Blackburn EH (1993) An alternative pathway for yeast telomere maintenance rescues est1-senescence. *Cell* 73: 347-360.

Lustig AJ (2003) Clues to catastrophic telomere loss in mammals from yeast telomere rapid deletion. *Nat Rev Genet* 4: 916-923.

Makovets S, Herskowitz I, Blackburn EH (2004) Anatomy and dynamics of DNA replication fork movement in yeast telomeric regions. *Molecular and cellular biology* 24: 4019-4031. doi:10.1128/mcb.24.9.4019-4031.2004

Margalef P, Kotsantis P, Borel V, Bellelli R, Panier S, Boulton SJ (2018) Stabilization of reversed replication forks by telomerase drives telomere catastrophe. *Cell* 172: 439-453 e414. doi:10.1016/j.cell.2017.11.047

Matmati S, Lambert S, Geli V, Coulon S (2020) Telomerase repairs collapsed replication forks at telomeres. *Cell Rep* 30: 3312-3322.e3313. doi:10.1016/j.celrep.2020.02.065

Mattarocci S, Shyian M, Lemmens L, Damay P, Altintas DM, Shi T, Bartholomew CR, Thoma NH, Hardy CF, Shore D (2014) Rif1 controls DNA replication timing in yeast through the pp1 phosphatase glc7. *Cell Rep* 7: 62-69. doi:10.1016/j.celrep.2014.03.010

Michelson RJ, Rosenstein S, Weinert T (2005) A telomeric repeat sequence adjacent to a DNA double-stranded break produces an anticheckpoint. *Genes Dev*:

Miller KM, Rog O, Cooper JP (2006) Semi-conservative DNA replication through telomeres requires taz1. *Nature* 440: 824-828. doi:10.1038/nature04638

Minca EC, Kowalski D (2010) Multiple rad5 activities mediate sister chromatid recombination to bypass DNA damage at stalled replication forks. *Mol Cell* 38: 649-661. doi:10.1016/j.molcel.2010.03.020

Miura T, Shibata T, Kusano K (2013) Putative antirecombinase srs2 DNA helicase promotes noncrossover homologous recombination avoiding loss of heterozygosity. *Proceedings of the National Academy of Sciences* 110: 16067-16072. doi:10.1073/pnas.1303111110

Moore A, Dominska M, Greenwell P, Aksenova AY, Mirkin S, Petes T (2018) Genetic control of genomic alterations induced in yeast by interstitial telomeric sequences. *Genetics* 209: 425-438. doi:10.1534/genetics.118.300950

Negrini S, Ribaud V, Bianchi A, Shore D (2007) DNA breaks are masked by multiple rap1 binding in yeast: Implications for telomere capping and telomerase regulation. *Genes Dev* 21: 292-302.

Noel JF, Wellinger RJ (2010) Abrupt telomere losses and reduced end-resection can explain accelerated senescence of smc5/6 mutants lacking telomerase. *DNA Repair (Amst)* 10: 271-282. doi:10.1016/j.dnarep.2010.11.010

Ortiz-Bazan MA, Gallo-Fernandez M, Saugar I, Jimenez-Martin A, Vazquez MV, Tercero JA (2014) Rad5 plays a major role in the cellular response to DNA damage during chromosome replication. *Cell Rep* 9: 460-468. doi:10.1016/j.celrep.2014.09.005

Pfander B, Moldovan GL, Sacher M, Hoege C, Jentsch S (2005) Sumo-modified pcna recruits srs2 to prevent recombination during s phase. *Nature* 436: 428-433. doi:10.1038/nature03665

Pfeiffer V, Crittin J, Grolimund L, Lingner J (2013) The tho complex component thp2 counteracts telomeric r-loops and telomere shortening. *EMBO J*: doi:10.1038/emboj.2013.217

Ribeyre C, Shore D (2012) Anticheckpoint pathways at telomeres in yeast. *Nat Struct Mol Biol*: doi:10.1038/nsmb.2225

Sfeir A, Kosiyatrakul ST, Hockemeyer D, MacRae SL, Karlseder J, Schildkraut CL, de LT (2009) Mammalian telomeres resemble fragile sites and require trf1 for efficient replication. *Cell* 138: 90-103. doi:10.1016/j.cell.2009.06.021

Shay JW, Wright WE (2019) Telomeres and telomerase: Three decades of progress. *Nat Rev Genet* 20: 299-309. doi:10.1038/s41576-019-0099-1

Shin S, Hyun K, Kim J, Hohng S (2018) Atp binding to rad5 initiates replication fork reversal by inducing the unwinding of the leading arm and the formation of the holliday junction. *Cell Rep* 23: 1831-1839. doi:10.1016/j.celrep.2018.04.029

Soudet J, Jolivet P, Teixeira MT (2014) Elucidation of the DNA end-replication problem in saccharomyces cerevisiae. *Mol Cell* 53: 954-964. doi:10.1016/j.molcel.2014.02.030

Strecker J, Stinus S, Caballero MP, Szilard RK, Chang M, Durocher D (2017) A sharp pif1-dependent threshold separates DNA double-strand breaks from critically short telomeres. *eLife* 6: doi:10.7554/eLife.23783

Teixeira MT (2013) Saccharomyces cerevisiae as a model to study replicative senescence triggered by telomere shortening. *Frontiers in oncology* 3: 101. doi:10.3389/fonc.2013.00101

Toulmay A, Schneiter R (2006) A two-step method for the introduction of single or multiple defined point mutations into the genome of saccharomyces cerevisiae. *Yeast* 23: 825-831. doi:10.1002/yea.1397

Ulrich HD (2001) The srs2 suppressor of uv sensitivity acts specifically on the rad5- and mms2-dependent branch of the rad6 pathway. *Nucleic Acids Res* 29: 3487-3494.

Ulrich HD (2011) Timing and spacing of ubiquitin-dependent DNA damage bypass. *FEBS Letters* 585: 2861-2867. doi:10.1016/j.febslet.2011.05.028

Vaurs M, Audry J, Runge KW, Géli V, Coulon S (2022) A proto-telomere is elongated by telomerase in a shelterin-dependent manner in quiescent fission yeast cells. *Nucleic Acids Res*: doi:10.1093/nar/gkac986

Voineagu I, Freudenreich CH, Mirkin SM (2009) Checkpoint responses to unusual structures formed by DNA repeats. *Mol Carcinog* 48: 309-318. doi:10.1002/mc.20512

Waga S, Stillman B (1998) The DNA replication fork in eukaryotic cells. *Annual Review of Biochemistry* 67: 721-751.

Wellinger RJ, Zakian VA (2012) Everything you ever wanted to know about saccharomyces cerevisiae telomeres: Beginning to end. *Genetics* 191: 1073-1105. doi:10.1534/genetics.111.137851

Xu Z, Fallet E, Paoletti C, Fehrmann S, Charvin G, Teixeira MT (2015) Two routes to senescence revealed by real-time analysis of telomerase-negative single lineages. *Nat Commun* 6: 7680. doi:10.1038/ncomms8680

Figures

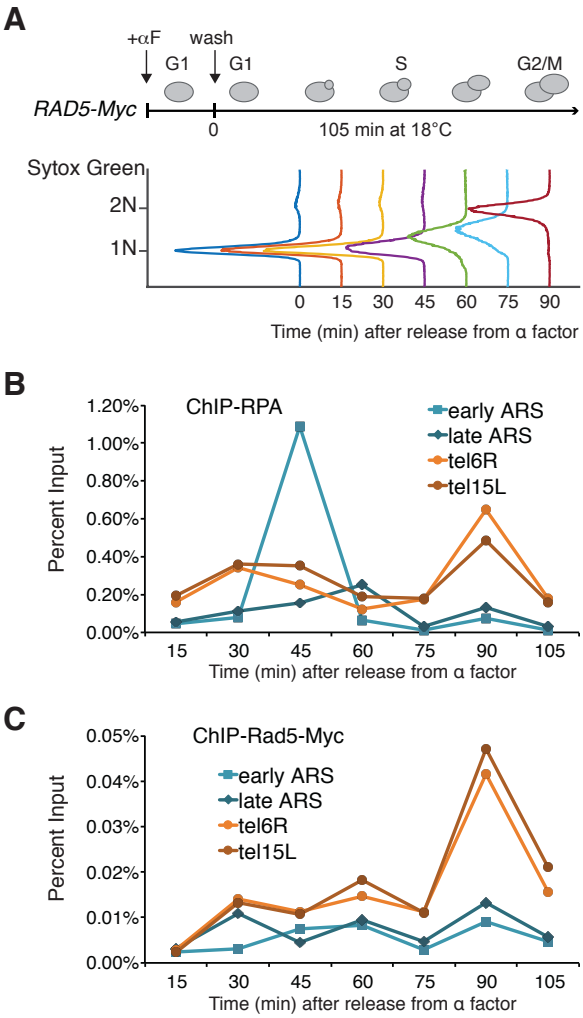

Figure 1- Rad5 is enriched at telomeres during their replication

(A) Cells with indicated genotype were synchronized using alpha factor and released at 18°C. Timepoints were taken every 15 minutes, and analyzed by flow cytometry using Sytox Green staining to quantify DNA content (1N or 2N). (B-C) The same samples were processed for ChIP and divided in half to immunoprecipitate either RPA (B) or Rad5-Myc (C). qPCR was used to determine the amount of two individual telomeres (6R and 15L), an early ARS, (*ARS607*), and a late ARS (ARS522) bound by RPA or Rad5-Myc. Results are expressed as a percentage of the input fraction.

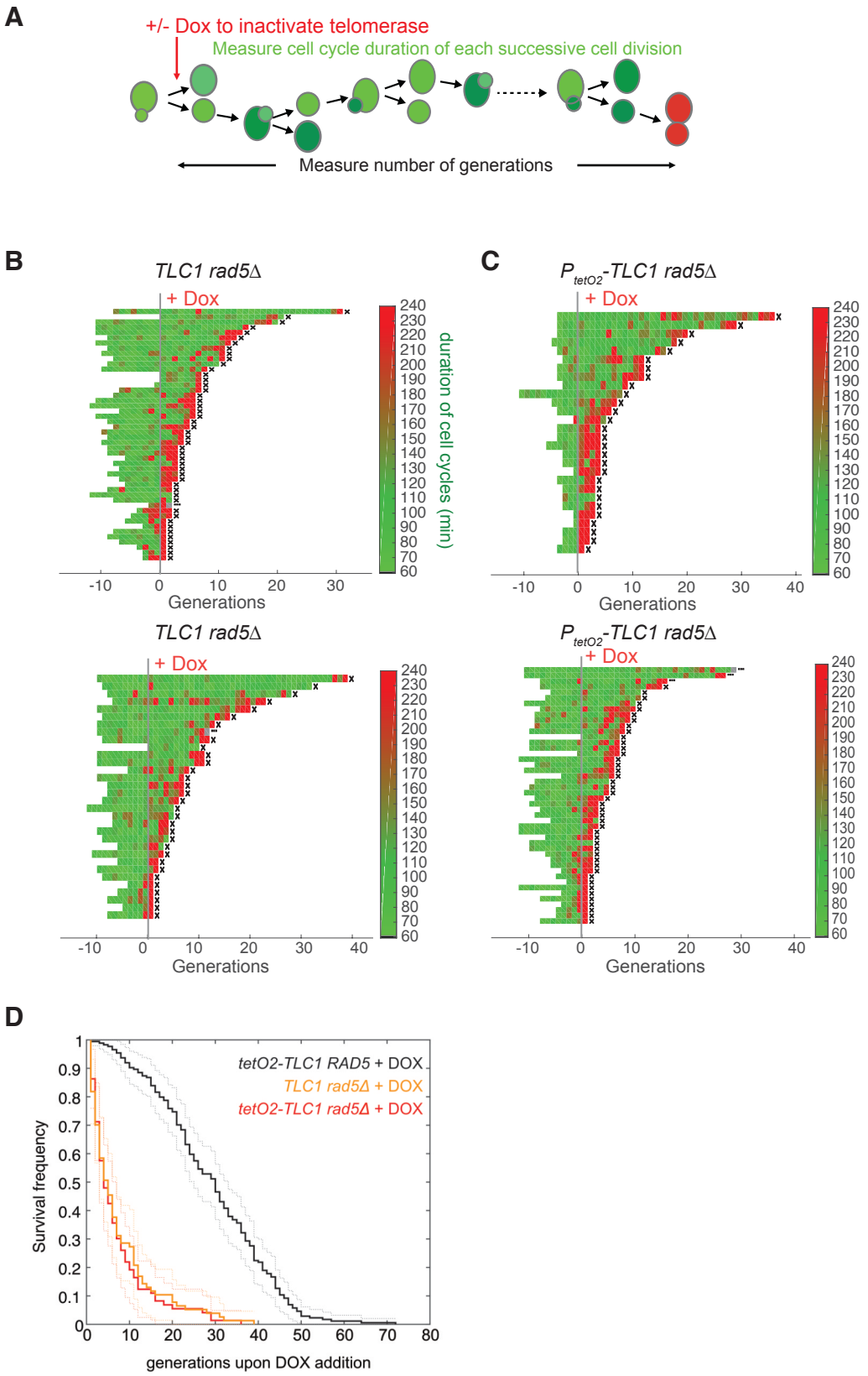
A
+/- Dox to inactivate telomerase
Measure cell cycle duration of each successive cell division
Measure number of generations
B
TLC1 rad5Δ
+ Dox
duration of cell cycles (min)
Generations
C
P tetO2-TLC1 rad5Δ
+ Dox
Generations
TLC1 rad5Δ
+ Dox
Generations
P tetO2-TLC1 rad5Δ
+ Dox
Generations
D
tetO2-TLC1 RAD5 + DOX
TLC1 rad5Δ + DOX
tetO2-TLC1 rad5Δ + DOX
Survival frequency
generations upon DOX addition

Figure 2: *rad5Δ* cells have a high mortality rate

(A) To evaluate growth capacity of cells in presence or absence of telomerase and in different genetic backgrounds, we measure the exact duration and the number of consecutive cell cycle in individual lineages. (B-C) Display of consecutive cell cycle durations of individual lineages with indicated genotypes grown in the microfluidic device obtained in one or two independent experiments using two independent transformants of *RAD5* deletion. Cells were monitored overnight before (-dox) and then for successive generations after (+dox) addition of doxycycline (30 µg/mL) to inactivate telomerase (designated generation 0). Each horizontal line is an individual cell lineage and each segment is a cell cycle. Cell cycle duration (min) is indicated by the color bar on the side. X at the end of the lineage indicates cell death, whereas an ellipsis (…) indicates that the cell was alive at the end of the experiment. (D) Survival frequency estimated by Kaplan-Meier method using pooled data from (B-C) for indicated genotypes. Dotted lines correspond to confidence bounds.

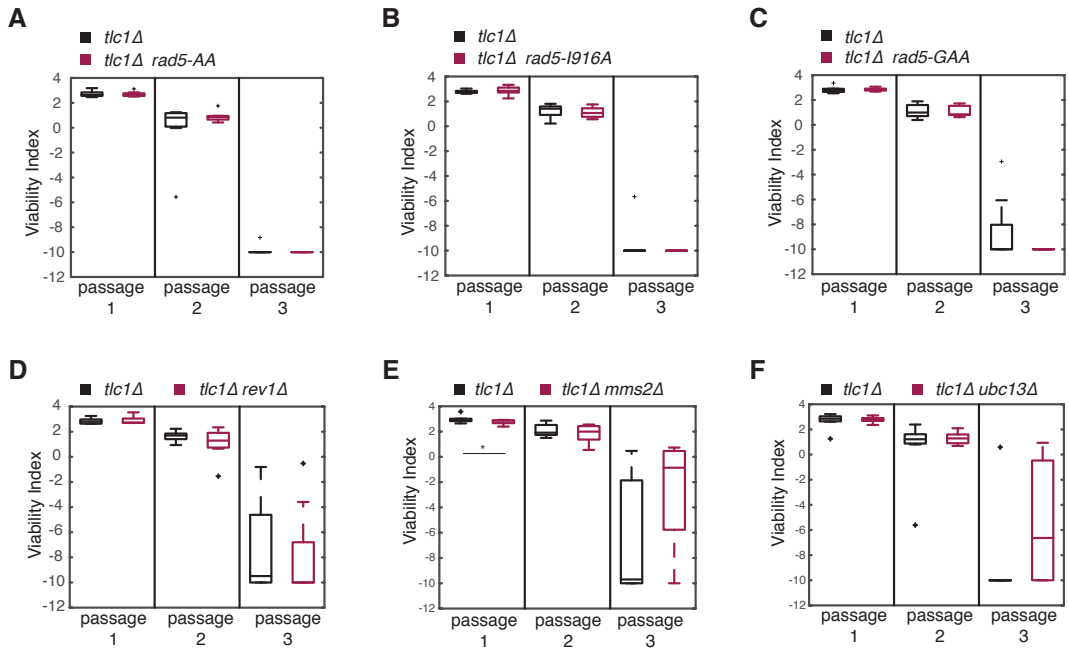

Figure 3- Rad5's role at telomeres does not involve helicase or ubiquitin ligase activities and is independent on the DDT pathway

(A-F) Quantitative assessment of senescence for strains with indicated genotypes. *tlc1Δ* spore-colonies derived from diploids *tlc1Δ /TLC1* combined with indicated mutations are genotyped and spotted on plates for three consecutive passages. Viability index reflects the capacity of forming colonies at each passage. Adjusted p-values were obtained by the Wilcoxon rank-sum test with a false discovery rate correction *p-value < 0.05, **p-value < 0.005.

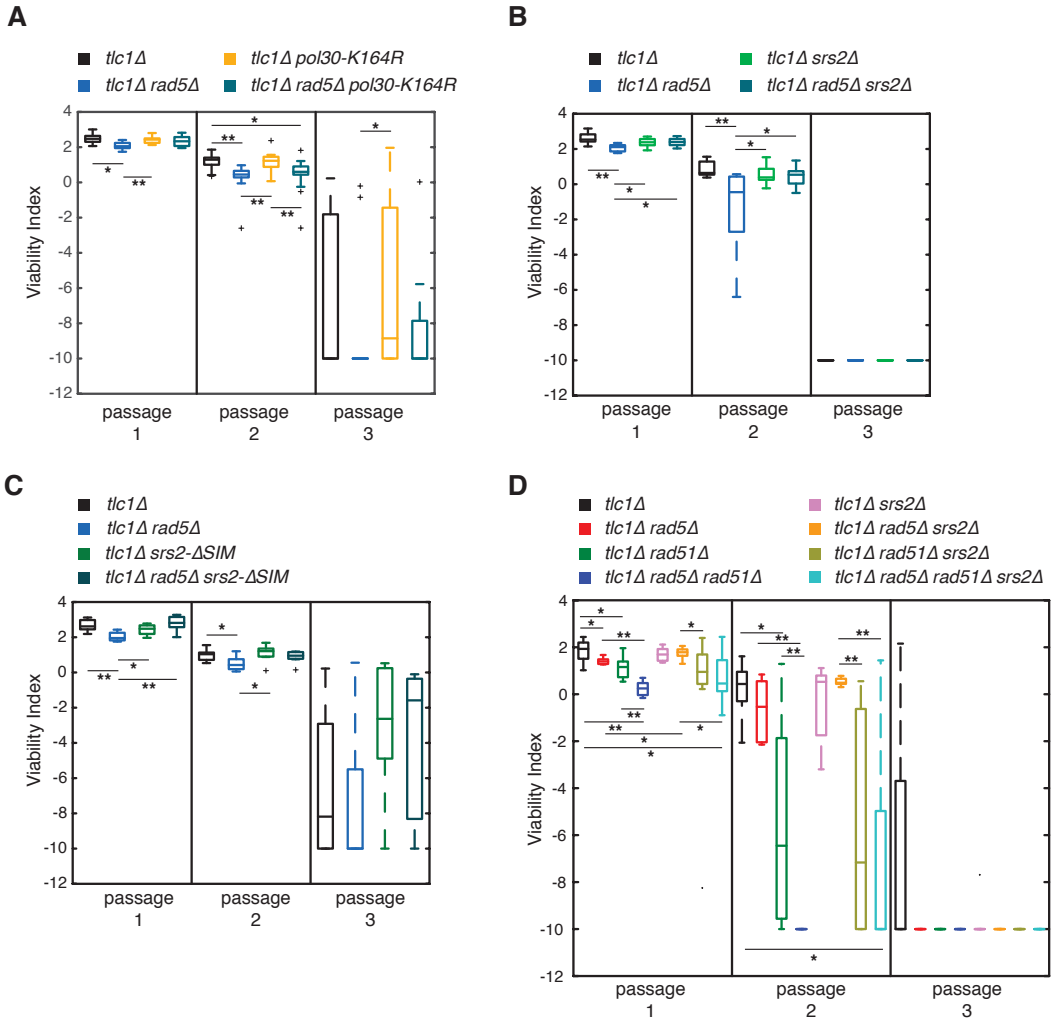

Figure 4- Rad5- and Rad51-dependent pathways both maintain cell viability in the absence of telomerase.

(A-D) Quantitative assessment of senescence for strains with indicated genotypes. *tlc1Δ* spore-colonies derived from diploids *tlc1Δ /TLC1* combined with indicated mutations are genotyped and spotted on plates for three consecutive passages. Viability index reflects the capacity of forming colonies at each passage. Adjusted p-values were obtained by the Wilcoxon rank-sum test with a false discovery rate correction *p-value < 0.05, **p-value < 0.005.

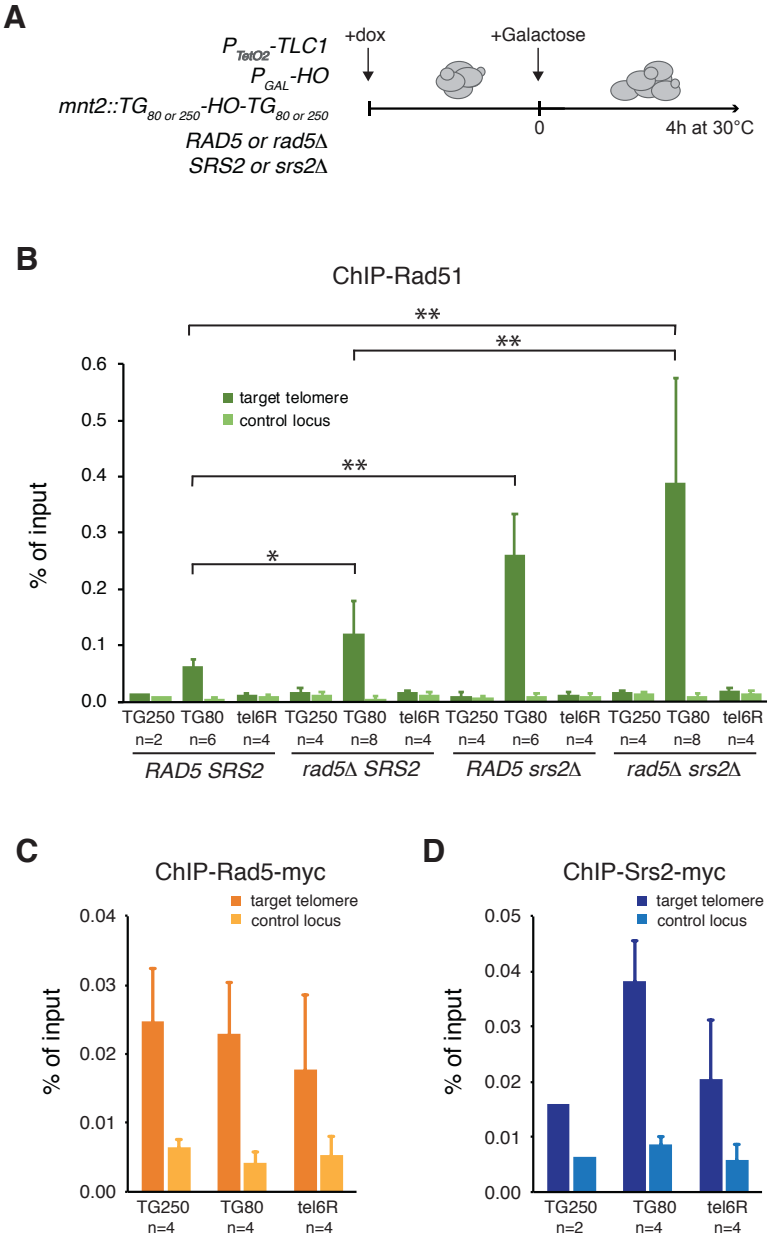

Figure 5- Rad51 recruitment to short telomeres is prevented by Rad5 and Srs2

(A) Cells with indicated genotype grown in the presence of Dox to repress telomerase and then shifted to galactose-containing media for 4 h to generate a telomeric extremity containing 80 bp or 250 bp of telomeric repeats, were harvested and chromatin was immunoprecipitated with anti-Rad51 antibodies (B) The association of Rad51 with the newly generated telomere (TG250 or TG80) or with an internal control locus (*PDZ1*) was quantified by qPCR. An unaffected telomere (tel6R) was also assessed in the strain harboring the

critically short telomere TG80 and its association with Rad51 was evaluated together with *ACT1* control locus. All data are depicted as mean + SD of n independent experiments (described in Supplementary Figure 5). p-values were obtained from two-tailed Student's t-tests (*$p < 0.05$, **$p < 0.01$). (C-D) Cells as in (A) expressing *RAD5-MYC* (C) or *SRS2-MYC* (D) and chromatin immunoprecipitated with anti-Myc antibodies. The association of Rad5-Myc or Srs2-Myc with the newly generated telomere (TG250 or TG80), an unaffected telomere (tel6R) and a control internal locus (*PDZ1*) was quantified by qPCR. Legends as in (B).

Supplementary Figures and Tables

Rad5 and Rad51 act at telomeres through two partially distinct pathways

Henninger et al.

Supplementary Figure 1 - Rad5 localizes to telomeres during their replication

Supplementary Figure 2 - cells deleted for RAD5 have a high mortality rate

Supplementary Figure 3 - Effects of mutations in Rad5 and DDT components

Supplementary Figure 4 - Penetrance of DDT mutations

Supplementary Figure 5 - Individual ChIP results for Figure 4

Supplementary Table 1: Average duration of cell cycles and mortality rates per cell division calculated for indicated experimental conditions.

Supplementary Table 2: Strains used in this study

Supplementary Table 3: Primers used in this study

Supplementary Figures

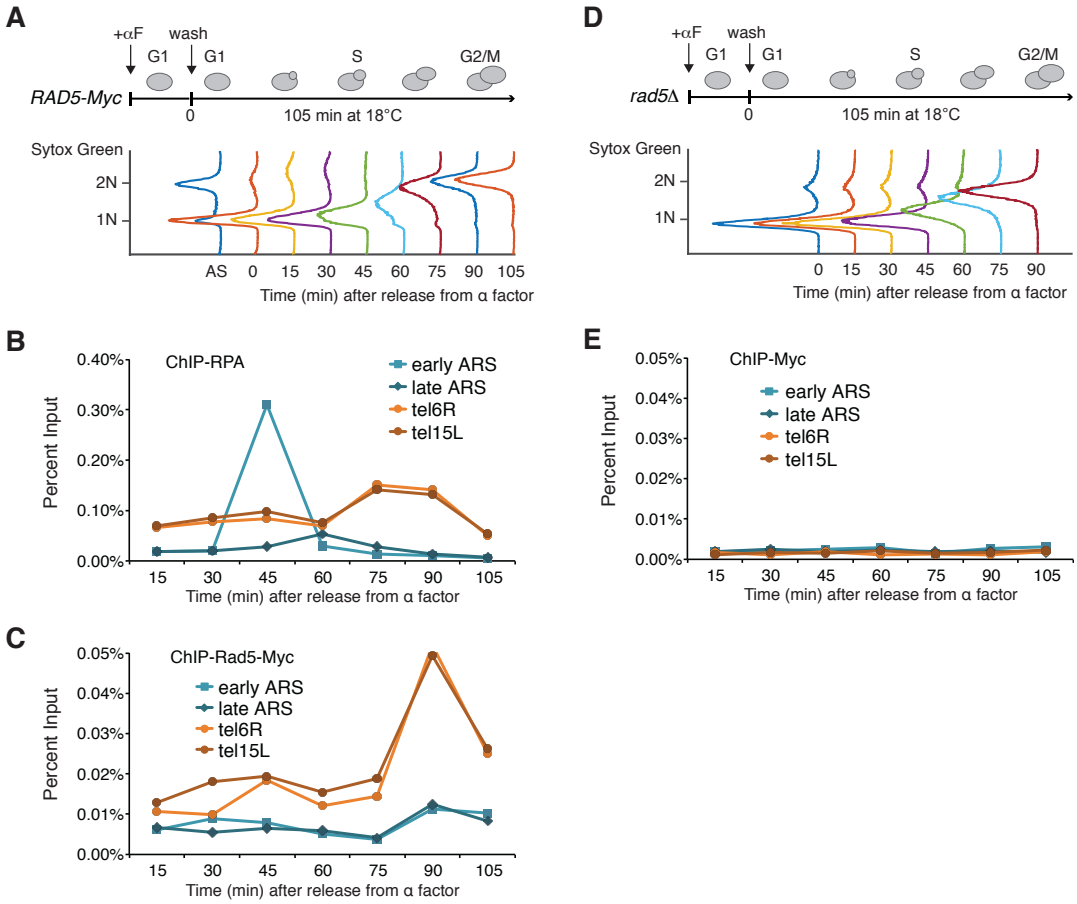

Supplementary Figure 1 - Rad5 localizes to telomeres during their replication

(A-C) Biological replicate of experiment shown in Figure 1A-C. (A) Cells with indicated genotype were synchronized using alpha factor and released at 18 °C. Timepoints were taken every 15 minutes, and analyzed by flow cytometry to quantify DNA content (1N or 2N). (B-C) The same samples were processed for ChIP and divided in half to immunoprecipitate either RPA (B) or Rad5-Myc (C). qPCR was used to determine the amount of two individual telomeres (6R and 15L), an early ARS, (ARS 607), and a late ARS (ARS522) bound by RPA or Rad5-Myc. Results are expressed as a percentage of the input fraction. (D-E) Similar to (A) and (C) with *rad5Δ* cells, as negative control.

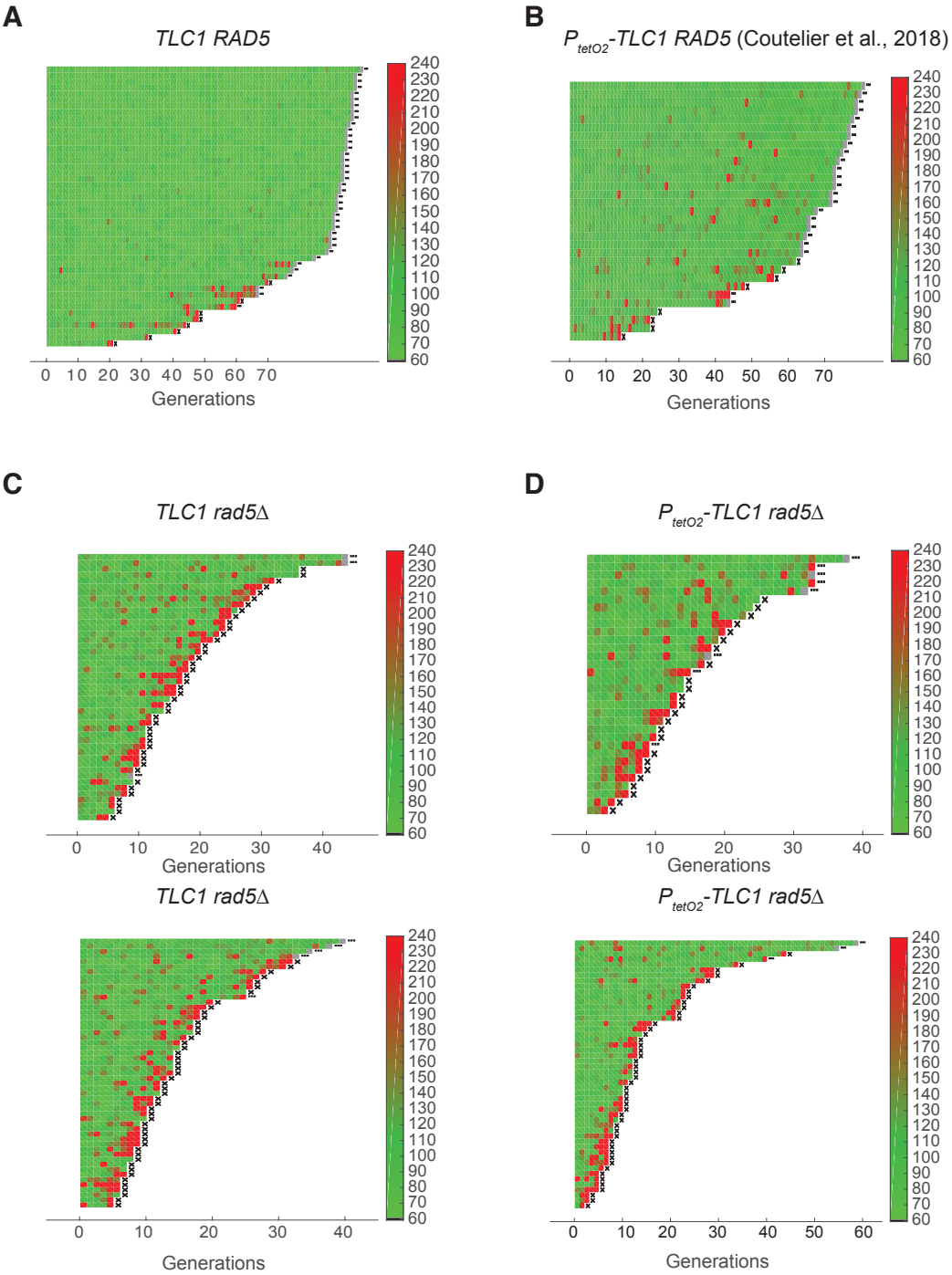
A
TLC1 RAD5
B
P_{tetO2}-TLC1 RAD5 (Coutelier et al., 2018)
C
TLC1 rad5Δ
D
P_{tetO2}-TLC1 rad5Δ
TLC1 rad5Δ
P_{tetO2}-TLC1 rad5Δ
Generations
240
230
220
210
200
190
180
170
160
150
140
130
120
110
100
90
80
70
60

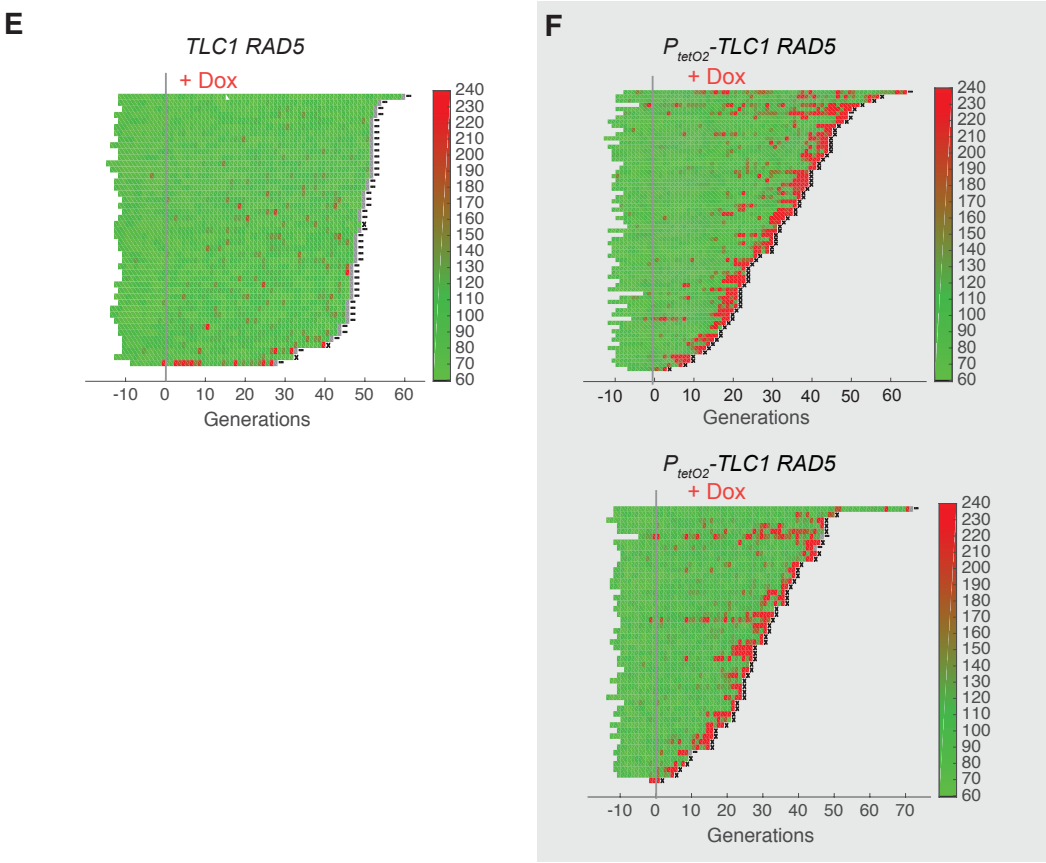

Supplementary Figure 2 - cells deleted for RAD5 have a high mortality rate

Display of consecutive cell cycle durations of individual lineages with indicated genotypes grown in the microfluidic device obtained in one or two independent experiments using two independent transformants of *RAD5* deletion, when applicable. In (B), data is taken from (Coutelier H et al, 2018, Xu Z et al, 2015). Cells were monitored overnight before (-dox) and then for successive generations after (+dox) addition of doxycycline (30 µg/mL) to inactivate telomerase (designated generation 0). In experiments in which doxycycline is not added, 0 corresponds to the beginning of the movie after injection of cells and invasion of microcavities. Each horizontal line is an individual cell lineage and each segment is a cell cycle. Cell cycle duration (min) is indicated by the color bar on the side. X at the end of the lineage indicates cell death, whereas an ellipsis (…) indicates that the cell was alive at the end of the experiment.

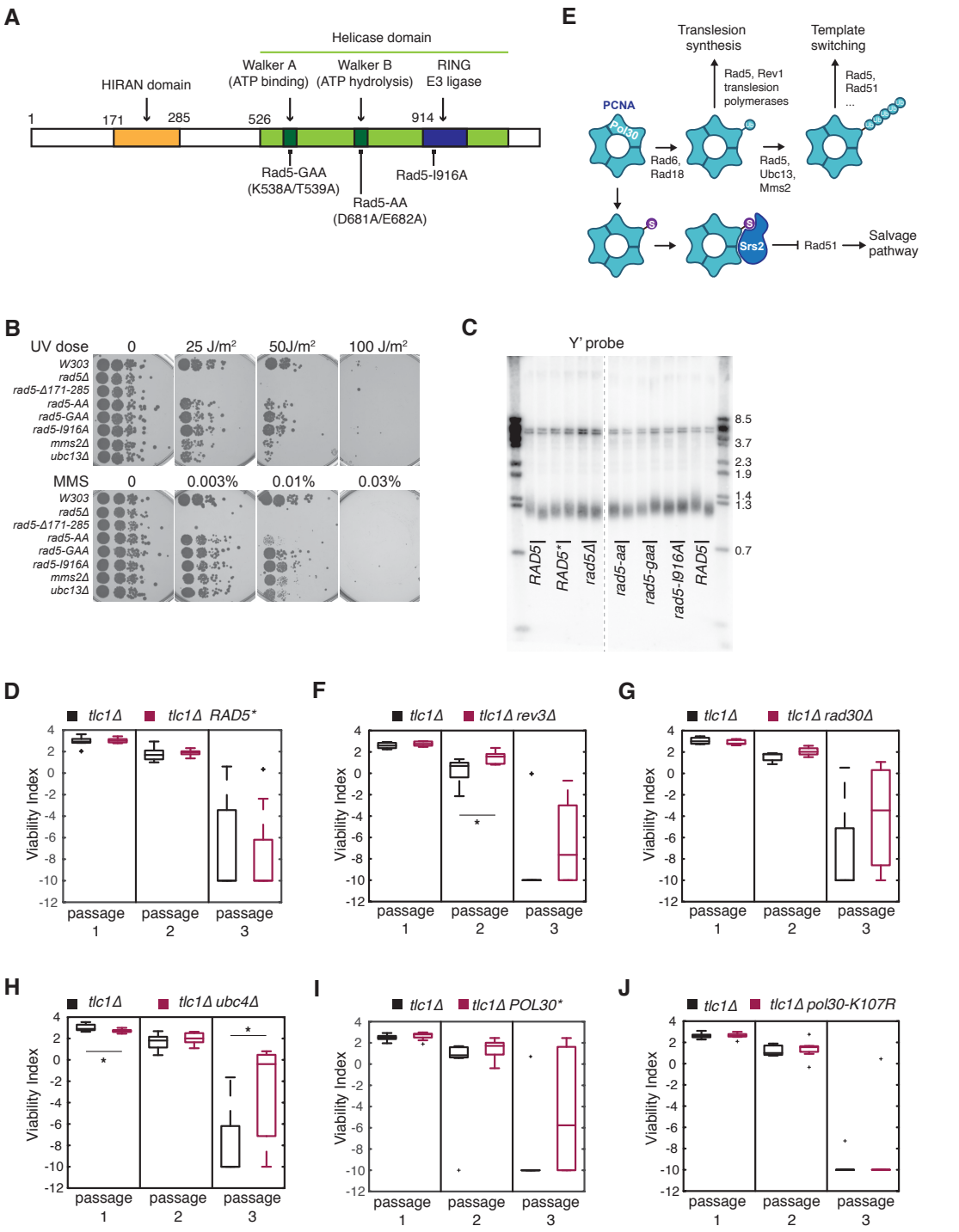

Supplementary Figure 3 - Effects of mutations in Rad5 and DDT components

(A) The Rad5 helicase contains a putative DNA-binding HIRAN domain (in orange), and an E3 ligase domain (blue) embedded in a SWI/SNF2 family helicase domain (green). The walker A and B motifs are depicted in dark green. (B) UV spot assays were performed with indicated *rad5* mutants. For each strain, 50,000 cells were plated in the most concentrated

spot, followed by 10-fold serial dilutions. Then plates were subjected to UV at 0, 5, 10 or 25 J/m2. Plates were incubated for 48 hours. (C) Southern blot analysis was performed on various *rad5* mutants using 250 ng of DNA from each strain. DNA was digested with *Xho* I, separated on a 1.2% agarose gel, and the blot was probed with a probe for Y' elements. (D, F-J) Quantitative senescence assays were performed as in Figure 2, for indicated genotypes. * stands for *RAD5-3'-UTR::HIS3MX6* and *POL30-3'-UTR::kLEU2*. (E) Schematic of the DNA Damage Tolerance pathway (DDT) operating when replication fork encounters a DNA lesion. The DDT is initiated by the Rad6/Rad18 ubiquitin ligase, which mono-ubiquitylates Pol30 (PCNA) on K164. The mono-ubiquitylation of Pol30 stimulates error-prone translesion synthesis (TLS) by TLS polymerases (Pols), a process that involves Rad5 helicase activity. Alternatively, the E3 ligase Rad5, working with E2 ligase complex Mms2/Ubc13, poly-ubiquitylates Pol30 on K164. This poly-ubiquitylation leads to template switching, which is an error-free process assisted by Rad5 and possibly Rad51. In another branch of the pathway, Srs2 helicase is recruited to SUMO-K164-Pol30, which blocks the activity of Rad51 by removing Rad51 filaments. Because the absence of Srs2 suppresses viability of *rad5Δ* cells, this branch is called "salvage pathway".

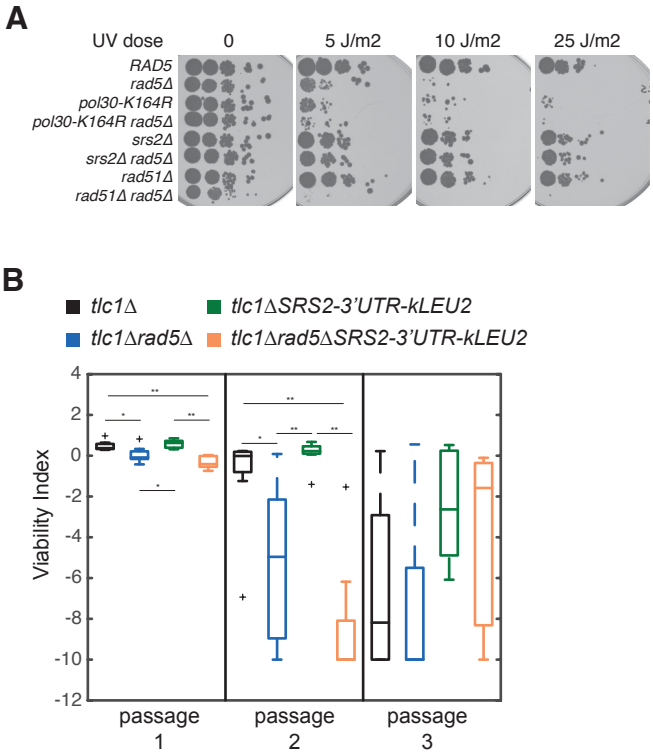

Supplementary Figure 4 - Penetrance of DDT mutations

(A) UV spot assays were performed with indicated mutants. For each strain, 50,000 cells were plated in the most concentrated spot, followed by 10-fold serial dilutions. Then plates were subjected to UV at 0, 5, 10 or 25 J/m2. Plates were incubated for 48 hours. (B) Quantitative senescence assay as in Figure 2 for indicated genotypes. *SRS2-3'UTR-kLEU2* stands for the *SRS2* allele in which the *kLEU2* marker is inserted in the 3'UTR of *SRS2* (used to construct *srs2ΔSIM*).

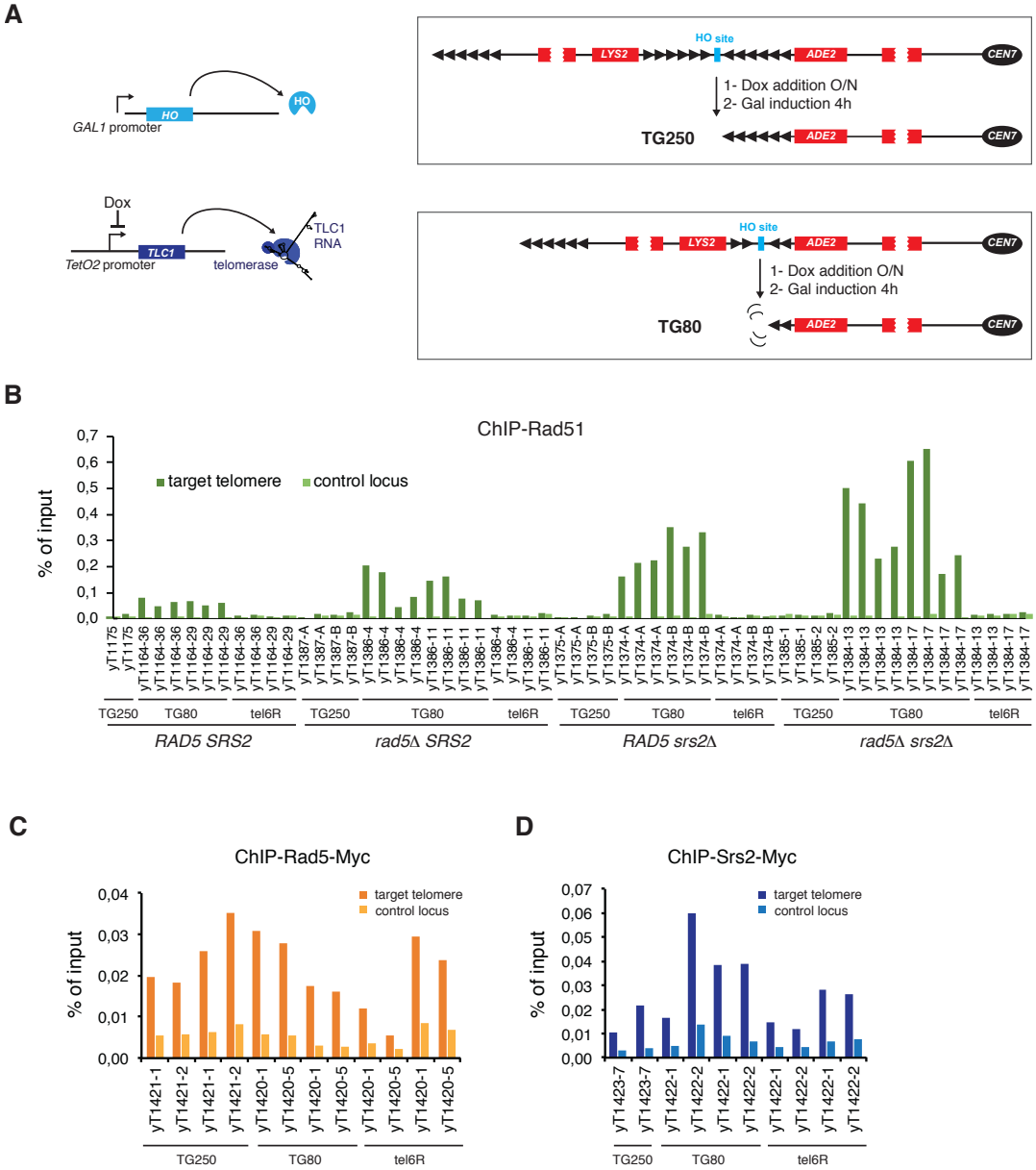

Supplementary Figure 5 - Individual ChIP results for Figure 4

Schematic representation of the experiment to induce a *de novo* critically short telomere (TG80) or a normal length telomere (TG250). Strains in this experiment contain a unique site for HO endonuclease, flanked by a variable number of telomeric repeats. This construct is embedded within a subtelomeric region of arm 7L, containing no essential genes from there to the telomeres. Cells also contain *TLC1*, encoding for telomerase template RNA subunit, under the control of a promoter repressible by addition of doxycycline (Dox) to the media. To induce a *de novo* telomere of controlled length, cells are first pre-incubated overnight

(O/N) in Dox, and then shifted for 4h into Galactose-containing media in presence of Dox, to induce the expression of endonuclease HO. This generates a new telomere containing either 250 or 80 bp of TG1-3 repeats (TG250 and TG80, respectively, depending on the strain). CEN7, centromere of chromosome 7; telomeric repeats are represented by black arrow heads, flanking markers *LYS2* and *ADE2* are depicted. (B-D) ChIP results shown in Figure 4 were obtained by averaging data shown obtained for indicated independent strains and clones (see Appendix Table 1).

Supplementary Table 1: Average duration of cell cycles and mortality rates per cell division calculated for indicated experimental conditions.

strain/treatment	average cell cycle length (min)	mortality rate[1]	
TLC1 RAD5	76.91 (+/- 0.48)	<0.0021	
TLC1 RAD5 + Dox	87.22 (+/- 0.49)	<0.0021	
TLC1 rad5Δ	105.44 (+/- 1.47)	0.0594	(0.0489-0.0719)
TLC1 rad5Δ + Dox	116.43 (+/- 1.85)	0.0675	(0.0571 - 0.0797)
tetO2-TLC1 RAD5	90.70 (+/- 0.87)	<0.0041	
tetO2-TLC1 RAD5+ Dox	101.93 (+/- 0.88)	0.0342	(0.0295 - 0.0396)
tetO2-TLC1 rad5Δ	105.31 (+/- 1.96)	0.0623	(0.0504 - 0.0767)
tetO2-TLC1 rad5Δ + Dox	118.47 (+/- 2.65)	0.1186	(0.0831 - 0.1668)

[1]The mortality rate is calculated as the fraction of cell deaths over total number of cell divisions among lineages, and the 95% confidence interval of a proportion was determined using the Wald method.

Supplementary Table 2: Strains used in this study

Strain	Figure	Genotype
G49 (W303)[#]	S2	*Mat a ura3-1 trp1-1 leu2-3,112 his3-11,15 can 1-100 RAD5*
yT752	1, S1	G49 *bar1::kLEU2 tlc1::KANMX6-*P_{TetO2}*-TLC1 rad5::His3*
yT1185	1, S1	G49 *bar1::kLEU2 tlc1::KANMX6-*P_{TetO2}*-TLC1 rad5::RAD5-13xMYC-TRP1*
yT769		*Mat α ura3-1 trp1-1 leu2-3,112 his3-11,15 can 1-100 RAD5 tlc1::PralphaNat pCEN-ARS-TRP1-TLC1 (pSD107)*
yT528	S2	*Mat α ura3-1 trp1-1 leu2-3,112 his3-11,15 can 1-100 RAD5 ADE2 LYS2 cdc10::CDC10-mCherry-kanMX tlc1::HIS3MX6-PtetO2-TLC1*
yT657	2, S2	G49 *rad5::HIS3MX6 tlc1-kanMX-PtetO2-TLC1*
yT649*	2, S2, S3, 4, S4	G49 *rad5::HIS3MX6*
yT650*	3, S3	G49 *mms2::HIS3MX6*
yT651	S3	G49 *ubc4::HIS3MX6*
yT652*	3, S3	G49 *ubc13::HIS3MX6*
yT656*	3, S3	G49 *RAD5-3'-UTR::HIS3MX6*
yT695*	3, S3	G49 *rad5-GAA-3'-UTR::HIS5*
yT696*	3, S3	G49 *rad5-I916A-3'-UTR::HIS5*
yT717*	3	G49 *POL30-3'-UTR::kLEU2*
yT745*	3, S3	G49 *rad5-AA-3'-UTR::HIS5*
yT749*	3	G49 *pol30-K107R-3'-UTR::kLEU2*
yT755*	S3	G49 *rad30::HIS3MX6*
yT756*	3, S3	G49 *rev1::HIS3MX6*
yT757*	S3	G49 *rev3::HIS3MX6*
yT758*	4	G49 *rad5::HIS3 pol30-K164R-3'-UTR::kLEU2*
yT747*	4, S4	G49 *pol30-K164R-3'-UTR::kLEU2*
yT800	4, S4	G49 *srs2::kLEU2*
yT801*	4, S4	G49 *srs2::kLEU2 rad5::HIS3MX6*
yT811	S4	G49 *rad5::RAD5-13xMYC-TRP*
yT868	4, S4	G49 *rad51::kLEU2 rad5::HIS3*
yT898	4, S4	G49 *rad51::kLEU2*
yT1026	4, S4	*Mata/alpha ura3-1/ura3-1 trp1-1/trp1-1 leu2-3,112/leu2-3,112 his3-11,15/his3-11,15 can1-100/can1-100 TLC1/tlc1::PralphaNat RAD5/rad5::HIS3 SRS2/srs2::TRP1 RAD51/rad51::kLEU2*
yT860	S4	G49 *SRS2-3'-UTR-kLEU2*
yT866	4	G49 *srs2-ΔSIM-3'-UTR-kLEU2*
yT867	4	G49 *rad5::HIS srs2-ΔSIM-3'-UTR-kLEU2*
yT1164	5, S5	G49 *leu2::*P_{GAL}*-HO mat1::loxP ade2::loxP lys2::loxP mnt2::LYS2 tlc1::HIS3MX6-*P_{TetO2}*-TLC1 mnt2::TG80-HO-CA80 ADE2*
yT1386	5, S5	G49 *leu2::*P_{GAL}*-HO mat1::loxP ade2::loxP lys2::loxP mnt2::LYS2 tlc1::HIS3MX6-*P_{TetO2}*-TLC1 mnt2::TG80-HO-CA80 ADE2 rad5::TRP1*
yT1374	5, S5	G49 *leu2::*P_{GAL}*-HO mat1::loxP ade2::loxP lys2::loxP mnt2::LYS2 tlc1::HIS3MX6-*P_{TetO2}*-TLC1 mnt2::TG80-HO-CA80 ADE2 rad5::TRP1 srs2::HPH*
yT1384	5, S5	G49 *leu2::*P_{GAL}*-HO mat1::loxP ade2::loxP lys2::loxP mnt2::LYS2 tlc1::HIS3MX6-*P_{TetO2}*-TLC1 mnt2::TG80-HO-CA80 ADE2 rad5::TRP1 srs2::HPH rad5::TRP1*
yT1175	5, S5	G49 *leu2::*P_{GAL}*-HO mat1::loxP ade2::loxP lys2::loxP mnt2::LYS2 tlc1::HIS3MX6-*P_{TetO2}*-TLC1 mnt2::TG250-HO-CA250 ADE2*
yT1387	5, S5	G49 *leu2::*P_{GAL}*-HO mat1::loxP ade2::loxP lys2::loxP mnt2::LYS2 tlc1::HIS3MX6-*P_{TetO2}*-TLC1 mnt2::TG250-HO-CA250 ADE2 rad5::TRP1*
yT1375	5, S5	G49 *leu2::*P_{GAL}*-HO mat1::loxP ade2::loxP lys2::loxP mnt2::LYS2 tlc1::HIS3MX6-*P_{TetO2}*-TLC1 mnt2::TG250-HO-CA250 ADE2 srs2::HPH*

yT1385	5, S5	G49 *leu2::P_{GAL}-HO mat1::loxP ade2::loxP lys2::loxP mnt2::LYS2 tlc1::HIS3MX6-P_{TetO2}-TLC1 mnt2::TG250-HO-CA250 ADE2 srs2::HPH rad5::TRP1*
yT1420	5, S5	G49 *leu2::P_{GAL}-HO mat1::loxP ade2::loxP lys2::loxP mnt2::LYS2 tlc1::HIS3MX6-P_{TetO2}-TLC1 mnt2::TG80-HO-CA80 ADE2 RAD5-Myc-TRP1*
yT1421	5, S5	G49 *leu2::P_{GAL}-HO mat1::loxP ade2::loxP lys2::loxP mnt2::LYS2 tlc1::HIS3MX6-P_{TetO2}-TLC1 mnt2::TG250-HO-CA250 ADE2 RAD5-Myc-TRP1*
yT1422	5, S5	G49 *leu2::P_{GAL}-HO mat1::loxP ade2::loxP lys2::loxP mnt2::LYS2 tlc1::HIS3MX6-P_{TetO2}-TLC1 mnt2::TG80-HO-CA80 ADE2 SRS2-Myc-TRP1*
yT1423	5, S5	G49 *leu2::P_{GAL}-HO mat1::loxP ade2::loxP lys2::loxP mnt2::LYS2 tlc1::HIS3MX6-P_{TetO2}-TLC1 mnt2::TG250-HO-CA250 ADE2 SRS2-Myc-TRP1*

[#]: Obtained from M. Lisby

*: These strains were crossed with yT769 to generate diploids for senescence spot assays.

Supplementary Table 3: Primers used in this study

Name	Sequence
oT230 deletion of *RAD5* (yT649, yT752, yT867 yT1190)	5′-TAC AAA GTT ACA TTA TCA AAA GGC CTT AGA AAC ACA CCT AAA GTC TTA CAG TAT CAC AAT CGG ATC CCC GGG TTA ATT AA-3′
oT231 deletion of *RAD5* (yT649, yT752, yT1190)	5′-AGT TCT TTC GGG TTG AAA ATA ATA ATA AAT AAA GTC TTT ATA TAT GAG TAT GTG GTA TGA GAA TTC GAG CTC GTT TAA AC-3′
oT234 deletion of *MMS2* (yT650)	5′-GTC GTG GTG AAA TTC TTA TTC TGT ATA TGC AAC GTA GAA GAA AGC AGC GTT TAC ACA AAA CGG ATC CCC GGG TTA ATT AA-3′
oT235 deletion of *MMS2* (yT650)	5′-TTG CTT GTA TAT ATG AGT GGC TTG GAA TGC TGC AAA TAC TGT TTA GGA AAA AGT AGA TAA GAA TTC GAG CTC GTT TAA AC-3′
oT612 deletion of *UBC4* (yT651)	5′-TAA ATT TCA CTG ACT ATA GAG TAC ATA CAT AAA CAA GCA TCC AAA AAA ACC GGA TCC CCG GGT TAA TTA A-3′
oT613 deletion of *UBC4* (yT651)	5′-AAT CCC ATA TAA ATC TTG CTT CTC TTT TTC AGC TGA GTA AGG ACT TCT GTG AAT TCG AGC TCG TTT AAA C-3′
oT608 deletion of *UBC13* (yT652)	5′-TTT TTC CAA TAT TAG CAA ATA AGG TCA GGT TCA TTG TAA CAT AGT TAG AAC GGA TCC CCG GGT TAA TTA A-3′
oT609 deletion of *UBC13* (yT652)	5′-GTA ATG ATA TAT ATT TAT ATA TTC AGT TGA GAA AAC TTA TAC AGA AAT GAG AAT TCG AGC TCG TTT AAA C-3′
oT637 marker HIS3MX6 at 3′ UTR of *RAD5* (yT656)	5′-TAT TTA TTA TTA TTT TCA ACC CGA AAG AAC TAA TTA TTC TTC AGC TAC TCG GAT CCC CGG GTT AAT TAA-3′
oT638 marker HIS3MX6 at 3′ UTR of *RAD5* (yT656)	5′-CAA CTT AAA AAT ACG GGT AAC GGA AAA GGA AGA TAA TAG AAG TTG CAT GAG AAT TCG AGC TCG TTT AAA C-3′
oT639 *rad5-GAA* point mutation (yT695)	5′-AGG GTG GCA TAT TAT CAG ATG AAA TGG GGT TGG GTG CAG CAG TGG CAG CGT ATT CTT TAG TTT TAT CTT G-3′
oT640 *rad5-I916A* point mutation (yT696)	5′-TCC AGA CAA TAA ATC GTT TCA GTC CTT AGA GTG CTC CGC CTG CAC AAC GGA ACC TAT GGA TTT GGA CAA G-3′
oT673 kLEU2 marker at 3′ UTR of *POL30* (yT717)	5′-AAT AAT AAA CAA AAA AAA AAC AGT AAA GTT TGT TTT AAA TGA AAA TAA ATC GGA TCC CCG GGT TAA TTA A-3′
oT674 kLEU2 marker at 3′ UTR of *POL30* (yT717)	5′-TCA CAC AAA AAG CTG ATA TTT AAC GCA TCT TAG TCT TTA TTT TCT TTG TTG AAT TCG AGC TCG TTT AAA C-3′
oT681 *rad5-AA* point mutation (yT745)	5′-TTC AGG CTT ATT TTC TGT CAA TTT TTA TCG CAT AAT AAT CGC CGC CGG TCA TAA CAT TAG AAA CAG AAC GAC AGT TAC AT-3′
oT 675 *pol30-K164R* point mutation (yT747)	5′-GTC CCA ATT GAG TGA TTC TAT TAA TAT CAT GAT CAC CCG Aga aac aat aaa gtt tgt agc tga cgg tga t-3′
oT679 *pol30-K107R* point mutation (yT749)	5′-ACA CAC CGG ATT CCA TCA TCT TAT TAT TTG AGG ATA CCA GGA AAG ACC GTA TAG CCG AAT ACT CTC TGA AAT TGA TGG AT-3′
oT770 *RAD30* deletion (yT755)	5′-TAG CGC AGG CCT GCT CAT TTT TGA ACG GCT TTG ATA AAA CAA GAC AAA GCC GGA TCC CCG GGT TAA TTA A-3′
oT771 *RAD30* deletion (yT755)	5′-ATC AGG ACG TTT TAG TTG CTG AAG CCA TAT AAT TGT CTA TTT GGA ATA GGG AAT TCG AGC TCG TTT AAA C-3′
oT774 *REV1* deletion (yT756)	5′-ACA GAT TTT CTC AAA ATA AAT CGA TAC TGC ATT TCT AGG CAT ATC CAG CGC GGA TCC CCG GGT TAA TTA A-3′
oT775 *REV1* deletion (yT756)	5′-TTC GCA AAC TGC GTG TTT ACT GTA TGC TGA AAT GTT TTT TTT TTT TTA ATG AAT TCG AGC TCG TTT AAA C-3′
oT778 *REV3* deletion (yT757)	5′-ATT TGA GTC AAT ACA AAA CTA CAA GTT GT GGC GAA ATA AAA TGT TTG GAA CGG ATC CCC GGG TTA ATT AA-3′
oT779 *REV3* deletion (yT757)	5′-ATA GAA ACA AAT AAC TAC TCA TCA TTT TGC GAG ACA TAT CTG TGT CTA GAG AAT TCG AGC TCG TTT AAA C-3′
oT436 *SRS2* deletion (yT800, yT810, yT1190)	5′-ATA ATT GTA CTC TGC ACT TTG AGT ATC ATT CCA ATT TGA TCT TTC TTC TAC CGG TAC TTA GGG ATA GCA ACG GAT CCC CGG GTT AA TTA A-3′
oT437 *SRS2* deletion (yT800, yT810, yT1190)	5′-CTC CTA TGT GCT TTA AAT AAA AAT TAT AAA CCG CCT CCA ATA GTT GAC GTA GTC AGG CAT GAA AGT GCT AGA ATT CGA GCT CGT TTA AAC-3′
oT352 Tagging Rad5-MYC or GFP (yT811, yT812, yT813, yT1185, yT1362)	5′-AGT TCT TTC GGG TTG AAA ATA ATA ATA AAT AAA GTC TTT ATA TAT GAG TAT GTG GTA TGA GAA TTC GAG CTC GTT TAA AC-3′

oT354 Tagging Rad5-MYC or GFP (yT811, yT812, yT813, yT1185, yT1362)	5′-GAC ACA GAC GAA GAC GAG AGA AGA AAA AGG AGA ATT GAA GAA ATC CAG ATG CTG TTT GAA CGG ATC CCC GGG TTA ATT AA-3′
oT965 kLEU2 marker at 3′ UTR of *SRS2* (yT860)	5′-GCC TGA CTA CGT CAA CTA TTG GAG GCG GTT TAT AAT TTT TAT TTA AAG CAC GGA TCC CCG GGT TAA TTA A-3′
oT966 kLEU2 marker at 3′ UTR of *SRS2* (yT860)	5′-CCA CAT TTC CAT GTA GTT CGT ATA CAA ACC CTA CCA GTA AAA TAA AAT TAG AAT TCG AGC TCG TTT AAA C-3′
oT964 *SRS2*-deltaSIM (yT866)	5′-TTT GGC TGA CGC AGC AAT GAA AAA GAC ACA GAA ATT TTC CAA AAA GGT GAA GAA TGA ACC TGC ATC AAG TTA GTA GCA CTT TCA TGC CTG ACT ACG TCA A-3′
oT323 Deletion of *RAD51* (yT868, yT898)	5′-TTC TTC TAT CTT CCG TAG TTT CCA TAT ACT AGT AGT TGA GTG TAG CGA CAC GGA TCC CCG GGT TAA TTA A-3′
oT324 Deletion of *RAD51* (yT868, yT898)	5′-GGA TGG AAA TGA AGA TAA AAA TGT ACG GAA CGC AAC CTA AGA AAA AGA GGG AAT TCG AGC TCG TTT AAA C-3′
oT1265 Telo15L Fwd	5′-ATC GTG GTT CGC TGT GGT AT-3′
oT1266 Telo15L Rev	5′-AAC CCT GTC CAA CCT GTC TCC-3′
oT1267 Telo6R Fwd	5′-TCC GAA CTC AGT TAC TAT TGA TGG AA-3′
oT1268 Telo6R Rev	5′-CGT ATG CTA AAG TAT ATA TTA CTT CAC TCC ATT-3′
oT1269 *ACT1* Fwd	5′-AAG CCG GTT TTG CCG G — 3′
oT1270 *ACT1* Rev	5′-TTG TGT CTT GGT CTA CCG ACG- 3′
oT1392 ARS607 Fwd	5′-TCT GAA CTG CAA ATT TTT GTC ATA-3′
oT1393 ARS607 Rev	5′-AGC CTT GTG CAG AAA GCA AA-3′
oT1394 ARS522 Fwd	5′-CGT TCG AAA ACC GGA TAT GT-3′
oT1395 ARS522 Rev	5′- CCC GAT GAC TAC GAG GCT AT-3′